Excitation Energy Transfer Dynamics and Excited-State Structure in Chlorosomes of *Chlorobium phaeobacteroides*

Jakub Pšenčík,*† Ying-Zhong Ma,*‡ Juan B. Arellano,*§ Jan Hála,† and Tomas Gillbro*

*Department of Chemistry, Biophysical Chemistry, Umeå University, S-901 87 Umeå, Sweden; †Department of Chemical Physics and Optics, Faculty of Mathematics and Physics, Charles University, 121 16 Prague, Czech Republic; ‡Department of Chemistry, University of California, Berkeley, California 94720-1460 USA; §Instituto de Recursos Naturales y Agrobiologia (CSIC), 37008 Salamanca, Spain

ABSTRACT The excited-state relaxation within bacteriochlorophyll (BChl) *e* and *a* in chlorosomes of *Chlorobium phaeobacteroides* has been studied by femtosecond transient absorption spectroscopy at room temperature. Singlet-singlet annihilation was observed to strongly influence both the isotropic and anisotropic decays. Pump intensities in the order of 10^{11} photons $\times$ pulse^{-1} $\times$ cm^{-2} were required to obtain annihilation-free conditions. The most important consequence of applied very low excitation doses is an observation of a subpicosecond process within the BChl *e* manifold (~200–500 fs), manifesting itself as a rise in the red part of the Q_y absorption band of the BChl *e* aggregates. The subsequent decay of the kinetics measured in the BChl *e* region and the corresponding rise in the baseplate BChl *a* is not single-exponential, and at least two components are necessary to fit the data, corresponding to several BChl *e*→BChl *a* transfer steps. Under annihilation-free conditions, the anisotropic kinetics show a generally slow decay within the BChl *e* band (10–20 ps) whereas it decays more rapidly in the BChl *a* region (~1 ps). Analysis of the experimental data gives a detailed picture of the overall time evolution of the energy relaxation and energy transfer processes within the chlorosome. The results are interpreted within an exciton model based on the proposed structure.

INTRODUCTION

Green photosynthetic bacteria involve two otherwise not closely related families, green filamentous (*Chloroflexaceae*) and green sulfur bacteria (*Chlorobiaceae*). The common property of both groups is the presence of similar extramembrane particles, called chlorosomes, attached to the inner side of cytoplasmic membrane (Blankenship et al., 1995; Olson, 1998). Chlorosomes serve as the main light-harvesting antennae and contain a large amount of bacteriochlorophyll (BChl) *c*, *d*, or *e* (depending on species). In addition, a minor amount of BChl *a* (~1% of total BChls) is present in the baseplate of the chlorosome envelope, which interfaces the entire chlorosome to the membrane. Chlorosomes also contain a substantial amount of carotenoids, whose exact location and function are still a matter of debate, but they are supposed to be in close contact with BChls (Psencik et al., 1994a; Frese et al., 1997; Arellano et al., 2000; Carbonera et al., 2001). A distinct feature of chlorosomes from other light-harvesting antennae is the formation of BChl *c*, *d*, and *e* aggregates, which are believed to form several rod-like elements, without considerable involvement of protein. Several models of the BChl organization in the rod have been proposed, among which the closely related structures reported by Holzwarth and Schaffner (1994), Steensgaard et al. (2000a), Prokhorenko et al. (2000), and van Rossum et al. (2001) are perhaps in best agreement with the available experimental data.

Chlorobium (*Cb.*) *phaeobacteroides* is a BChl *e* containing, strictly anaerobic green sulfur bacterium, which is able to survive at extremely low light conditions. It was even found in the Black Sea at a depth of 80–100 m, where the solar irradiance is lower than 0.003 μE $\times$ m^{-2} $\times$ s^{-1} (Overmann et al., 1992). The chlorosomes have to be thus very efficient in light harvesting. In the case of green sulfur bacteria, the photons absorbed by chlorosome pigments are transferred to BChl *a* in the baseplate only at low redox potentials, whereas in the presence of oxygen the excitation is quenched by quinones (Frigaard et al., 1997) and/or BChl radicals (van Noort et al., 1997) in a process that seems to protect reaction centers against reactive oxygen species. From the baseplate, the excitation is transferred to reaction centers in the cytoplasmic membrane, presumably via the so-called FMO protein complex.

So far there exist only few clear evidences about energy transfer within the BChl *c*, *d*, or *e* manifold. For an unique strain of *Cb. limicola* containing a mixture of BChl *c* and *d*, a 4-ps component corresponding to the energy transfer between these two types of pigments was resolved by single-photon-timing (SPT), however only at low temperature (Steensgaard et al., 2000b). Previously, a 5-ps transfer was observed by the same technique in the BChl *a*-free, BChl *c* containing chlorosomes of *Chloroflexus* (*Cf.*) *aurantiacus*, but it was not observed in untreated chlorosomes (Holzwarth et al., 1990). Both these reported transfer lifetimes are similar to the lifetime of the lowest exciton level of BChl *c* (≥5–6 ps) as determined by spectral hole burning at 4 K (Psencik et al., 1994b, 1998). Using femtosecond transient absorption (TA) technique, the only direct evidence about energy transfer within the main chlorosome BChl was an observation of a ~300-fs rise component for *Cf. aurantiacus* at low

Submitted May 15, 2002, and accepted for publication October 2, 2002.

Address reprint requests to Jakub Pšenčík, Faculty of Mathematics and Physics, Dept. of Chemical Physics and Optics, Charles University, Ke Karlovu 3, 121 16 Prague 2, Czech Republic. Tel.: 420-2-2191 1627; Fax: 420-2-2191 1249; E-mail: jakub.psencik@mff.cuni.cz.

0006-3495/03/02/1169/19 $2.00

temperature (Savikhin et al., 1996a). Other evidences of exciton relaxation and energy transfer processes within the chlorosome aggregates are indirect, based on a wide variety of decay components (in the order of 0.1–100 ps) obtained for BChls *c*, *d*, and *e* by means of various time-resolved spectroscopy techniques (Blankenship et al., 1995 and references therein, Savikhin et al., 1995, 1996b, 1998; Mimuro et al., 1996; Ma et al., 1996; Psencik et al., 1998; van Walree et al., 1999; Prokhorenko et al., 2000).

The energy transfer process from the aggregated BChls to the baseplate is much better characterized. In earlier SPT and TA studies, it has been found that this transfer can be described by a single time constant, with a value depending on the species (Holzwarth et al., 1990; Miller et al., 1991; Causgrove et al., 1992), growth conditions of the bacteria (Ma et al., 1996; Fetisova et al., 1996) and redox states (Causgrove et al., 1990; Wang et al., 1990; van Noort et al., 1997). However, using a two-color femtosecond pump-probe technique with the chlorosomes of *Cf. aurantiacus*, Savikhin et al. (1996b) observed a biexponential rise with lifetimes of 2–3 and 8–11 ps in the kinetics probed in the baseplate BChl *a*, after the excitation of the aggregated BChl *c*. This biphasic energy transfer feature was explained as due to the both intra-BChl *c* and BChl *c*→BChl *a* energy transfer steps based on the kinetic simulation (Savikhin et al., 1996b). Two discrete time constants were also found recently to be necessary in the description of the energy transfer in the isolated BChl *c* and *e* containing chlorosomes from *Cb. tepidum* and *Cb. phaeobacteroides*, respectively, using picosecond SPT technique (van Walree et al., 1999, Steensgaard et al., 2000b). This biphasic energy transfer was also found for *Cb. phaeobacteroides* in a comparative TA and SPT study (Psencik et al., 2002), and the nature of the two processes will be further addressed here. In particular, it is interesting to know whether these resolved transfer times are correlated with the presence of multiple, spectrally different pigment pools in the aggregated BChls and/or the baseplate, as proposed for some green bacteria (Blankenship et al., 1995 and references therein; Psencik et al., 1994b, 1998; Savikhin et al., 1995; Mimuro et al., 1996; Somsen et al., 1996; Steensgaard et al., 2002b; Melo et al., 2000; Carbonera et al., 2001) or only with the architecture of the chlorosome.

In this study, we applied two-color femtosecond TA technique to investigate systematically the excitation energy transfer within chlorosome BChls. Special care was dedicated to avoid the onset of exciton annihilation, which enabled us to reveal otherwise hidden energy transfer processes. The experimental data thus provide information about the excitation migration within and between the aggregates, and finally to BChl *a* in the baseplate. For the interpretation of the data we used a model based on the structure of Holzwarth and Schaffner (1994). We show that with minor changes, this model allows to better explain main features of the steady-state optical spectra and provide a good basis for interpretation of time-resolved data.

MATERIALS AND METHODS

Sample preparation

Growth of cells of *Cb. phaeobacteroides* strain CL1401 and isolation of chlorosomes were carried out as described previously (Arellano et al., 2000), and samples were kept at −20°C until use. All TA experiments were performed on isolated chlorosomes diluted with 50 mM Tris-HCl buffer (pH 8.0) containing 2 M NaSCN to an absorbance ranging from 0.25 to ~3.5 per mm at the respective BChl *e* Q_y maxima, depending on the pump-probe wavelengths. 1-mm glass cuvettes were used and the chlorosomes were incubated with 20–25 mM sodium dithionite for 2 h before the measurements to achieve anaerobic conditions. Absorption spectra were measured before and after the experiments to ensure that no degradation occurred during the data acquisition.

Femtosecond TA

Two-color femtosecond TA kinetics were measured using a setup based on a mode-locked Ti:sapphire femtosecond oscillator (Tsunami, Spectra Physics, Mountain View, CA) together with a Ti:sapphire regenerative amplifier (Spitfire, Positive Light, Los Gatos, CA) producing ~100-fs pulses centered around 800 nm at a repetition rate of 5 kHz. The output of the amplifier was split and the major part was used for pump pulse generation by frequency conversion in an optical parametric amplifier (OPA 800, Spectra Physics) to desired excitation wavelengths (505, 685, 715, or 745 nm). 505-nm pulses were further compressed by two SF14 prisms. Pulses of $\lambda \geq 685$ nm were used without compression. A white-light continuum generated in a sapphire plate by the minor part of the amplifier output was used as a probe pulse. The relative polarization of the pump beam with respect to the probe beam was set to the desired angle (54.7°, 0°, or 90°) by a Berek compensator (New Focus, Santa Clara, CA). The probe wavelength was selected after passing a monochromator with a bandwidth of 2.6–5.7 nm. Absorption changes were detected by silicon photodiodes. Excitation intensity was between $\sim 2 \times 10^{11}$ and 4×10^{14} photons $\times$ cm^{-2} $\times$ pulse^{-1}, and the spot size of the pump beam at the sample place was 0.5–0.7 mm. Beam intensity profile was measured by scanning a sharp blade mounted on a micrometer screw through the sample position and detecting the laser intensity behind the blade with a silicon photodiode. Spot size was determined at the point where the intensity equals to $1/e^2$ times the peak intensity. The cross correlation between the pump and probe pulses was ~150 fs and ~200 fs (full-width at half maximum (FWHM)) for the pump wavelengths at 505 and ≥685 nm, respectively. Deconvolution fitting of the isotropic and anisotropic kinetics, as well as the global lifetime analysis, were calculated using the Spectra program (S. Savikhin Software, Ames, IA).

EXPERIMENTAL RESULTS

Absorption and emission spectra of the *Cb. phaeobacteroides* chlorosomes at room temperature are shown in Fig. 1. The main absorption bands in the near infrared are the Q_y bands of BChl *e* and BChl *a*, at 714 and ~790 nm, respectively. The fluorescence emission spectra show bands at 742 and 808 nm, due to BChl *e* and BChl *a*, respectively. TA kinetics were measured upon excitation at 505 nm, 685 nm, 715 nm, and 745 nm, among which the kinetics excited at 685 nm were studied in a greater detail. Probe wavelengths ($\lambda_{det} \geq \lambda_{exc}$) were chosen to cover the major part of the BChl *e* and BChl *a* absorption and emission spectra (685–825 nm, Fig. 1). The kinetics are dominated by excited state absorption (ESA) at the high energy side of the BChl *e* Q_y absorption band, whereas photobleaching and/or stimulated

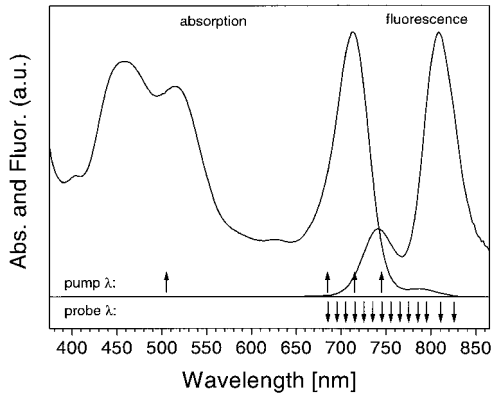

FIGURE 1 Steady-state absorption and fluorescence spectra of *Cb. phaeobacteroides* chlorosomes at room temperature. All pump and probe wavelengths used in this work are denoted in the bottom of the figure. Fluorescence spectrum was measured after incubation with 20 mM sodium dithionite for 2 h.

emission (PB/SE) prevail on longer wavelengths. The zero-crossing wavelength (isosbestic point), which separates these two regions, is located at ~700 nm.

Annihilation in BChl *e* manifold

Both the isotropic and anisotropic decays are strongly affected by exciton annihilation, and pump intensities in the order of 10^{11} photons $\times$ pulse^{-1} $\times$ cm^{-2} were required to obtain kinetics with negligible annihilation effect. An exact intensity is dependent on the excitation wavelength. For excitation at 715 nm, a pump intensity of $\sim 3 \times 10^{11}$ photons $\times$ pulse^{-1} $\times$ cm^{-2} was required to get annihilation-free kinetics, although it was sufficient to use 7×10^{11} photons $\times$ pulse^{-1} $\times$ cm^{-2} at 685 and 745 nm, regardless of sample optical density (OD). The effect of excitation intensity on isotropic decays of BChl *e* is illustrated in Fig. 2 *a*. Note that the decays were normalized to their maximal intensities, which makes the difference between decays measured at the two lowest pump intensities less pronounced due to their low signal-to-noise ratio. Further attenuation of the pump intensity by a factor of 2 led to a profile that is undistinguishable from the curve measured at 7×10^{11} photons $\times$ pulse^{-1} $\times$ cm^{-2} (not shown). Under the intensity of negligible annihilation, the amplitude of the TA signal was found to be typically less than 0.001 OD for a sample of ~1 OD at the absorption maximum. Due to the extremely low pump intensities used to obtain negligible annihilation, the experimental profiles exhibit a relatively low signal-to-noise ratio. Therefore, we cannot exclude the possibility that some residual contribution of annihilation is hidden within the relatively large noise, however, the effect is expected to be rather small. In addition, although the overall shape of the experimental profiles measured at given pump-probe wavelength combination were always well reproducible, the fitting parameters obtained for independent measurements were

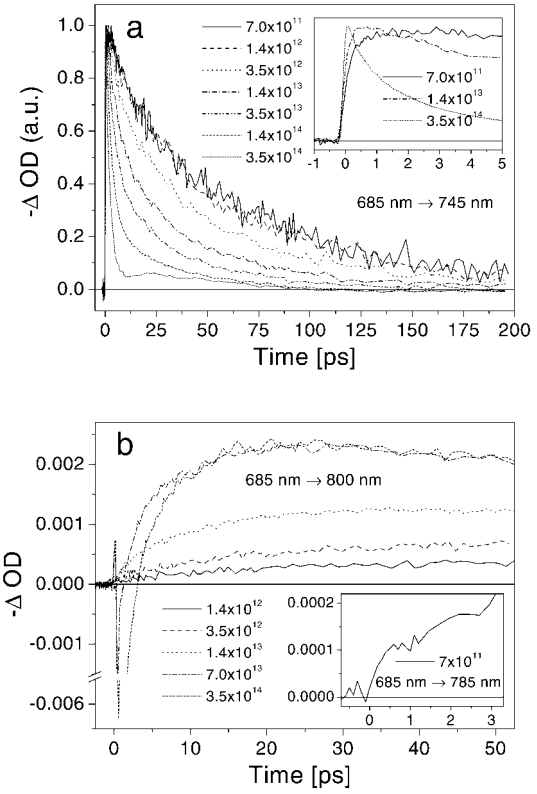

FIGURE 2 Pump-intensity dependence of the isotropic kinetics probed in BChl *e* at 745 nm (*a*) and in BChl *a* at 800 nm (*b*) upon excitation at 685 nm. Intensities are in photons $\times$ pulse^{-1} $\times$ cm^{-2}, and the sample OD was ~1 at the BChl *e* Q_y maximum. Inset in (*a*) shows three of the kinetics in the short timescale, and in (*b*) the first 4 ps of the isotropic kinetics probed in BChl *a* at 785 nm upon excitation at 685 nm under pump intensity of 7×10^{11} photons $\times$ pulse^{-1} $\times$ cm^{-2}, and the sample OD was ~3.5 at the BChl *e* Q_y maximum.

determined to be of standard deviations ±2–15%. To minimize the uncertainty in the estimation of the fitting parameters, 3–8 kinetic traces for each probe wavelength were measured independently upon excitation at 685 nm, and the parameters obtained from the best fits to the most representative profiles are presented.

The amplitude of the TA signal is linearly proportional to the pump intensity as it is $\leq 1 \times 10^{13}$ photons $\times$ pulse^{-1} $\times$ cm^{-2}. For a sample with ~1 OD per mm at 714 nm, the corresponding magnitudes of the TA amplitude are $\Delta OD \leq 0.01$, i.e., their upper limit is one order of magnitude larger than that associated with the annihilation-free signal. At even higher pump intensities, the annihilation led not only to acceleration of the isotropic decay but also to a nonmonotonic course of decay, similar to that observed for B800-850 antenna complexes of purple bacteria (Ma et al., 1997). Under the highest pump intensities used (~4×10^{14} photons $\times$ pulse^{-1} $\times$ cm^{-2}), the TA signal probed at certain wavelengths even exhibits positive ΔOD values during first 20 ps (not shown) after the initial fast decay, and the amplitude of the transient signal decreases with the pump intensity instead.

Rise in BChl *e*

Besides the apparent deceleration of the decay, the most striking effect observed for isotropic decays within the BChl *e* spectral region with the decrease of pump intensity was the appearance of a subpicosecond rise component for many combinations of sufficiently separated pump-probe wavelengths. Such a feature has never been observed previously for chlorosomes at room temperature, presumably due to the presence of annihilation to certain extent or insufficient separation between the pump and probe wavelengths. Previously, a rise was observed only for the chlorosomes from *Cf. aurantiacus* at 19–100 K, but it disappeared at higher temperatures (Savikhin et al., 1996a). From our experiments performed at 77 K on the chlorosomes from *Cb. phaeobacteroides*, we know that the rise in the kinetics measured at low temperatures is more pronounced and can be observed at higher pump intensities than those needed at room temperature (manuscript in preparation). This rise indicates an energy transfer within BChl *e* and can be resolved as long as the excitation intensity is equal to or below $\sim 10^{12} - 10^{13}$ photons $\times$ pulse^{-1} $\times$ cm^{-2} (depending on pump-probe wavelengths), but the time constant associated with this rise is intensity dependent (inset of Fig. 2 *a*). This dependence is negligible only at the pump intensity of $\sim 10^{11}$ photons $\times$ pulse^{-1} $\times$ cm^{-2}. In addition, the actual lifetime and amplitude of the rise depends on the pump-probe wavelength separation. Upon excitation at 685 nm, we could resolve the rise for $\lambda_{det} \geq 725$ nm, and with the red shift of the probe wavelength the lifetime increases from $\sim$200 to $\sim$500 fs (Table 1; Fig. 3). Excitation at 715 nm leads to relatively shorter rise lifetimes at respective probe wavelengths (Table 2; Fig. 4), and even more pronounced shortening was observed upon excitation at 745 nm. On the other hand, excitation in the Soret band leads to similar lifetimes as obtained for excitation at 685 nm and no rise could be resolved at $\lambda_{det} \leq 715$ nm.

Decay of BChl *e*

After the subpicosecond rise, the kinetics of BChl *e* probed at $\lambda_{det} \geq 700$ nm exhibit wavelength-dependent decays, characterized by gradual slowdown of the decay with increasing probe wavelength (Table 1; Fig. 3). In contrast to the initial rise, the change of pump wavelength has only moderate effect on the decay: the decay times resolved from the kinetics probed at a given wavelength appear often slower with shorter pump wavelength (Table 2; Fig. 4). Table 1 summarizes the fitting parameters of the kinetics measured upon excitation at 685 nm. In general, most of the kinetics can be fitted by a model function consisting of one rise and two decay components. Distinguishable improvement of the fits to the first 10 ps of the kinetics measured at $\lambda_{det} \leq 725$ nm, i.e., those close to the isosbestic point ($\sim$700 nm) and exhibiting more complicated shape, could be achieved by adding a fourth component, but it only gives a minor improvement of χ^2(<5%). For kinetics probed at $\lambda_{det} \geq 735$ nm, the addition of the fourth component leads to an indistinguishable χ^2(<1%). In addition, the difference between lifetimes obtained from the fitting using three and four components becomes smaller with the increase of the probe wavelength.

TABLE 1 Fitting parameters for the two-color isotropic kinetics measured upon excitation at 685 nm under a pump intensity of 7×10^{11} photons $\times$ pulse^{-1} $\times$ cm^{-2}

λ_{det} (nm)	Scan length (ps)	τ_1 (ps) (A_1)	τ_2 (ps) (A_2)	τ_3 (ps) (A_3)	τ_4 (ps) (A_4)
705	200	0.15 (52%)	2.7 (25%)	55 (23%)	–
		0.16 (49%)	*1.3 (21%)*	*25 (23%)*	*118 (7%)*
715	200	0.82 (26%)	17.2 (40%)	99 (34%)	–
		0.53 (12%)	*2.6 (25%)*	*28 (41%)*	*129 (22%)*
725	200	0.23 (−21%)	18.8 (53%)	103 (47%)	–
		0.29 (−27%)	*5.7 (15%)*	*34 (58%)*	*161 (25%)*
735	200	0.36 (−30%)	18.2 (49%)	92 (51%)	–
		0.39 (−32%)	*7.8 (18%)*	*44 (69%)*	237 (14%)
745	200	0.42 (−39%)	18.5 (37%)	82 (63%)	–
		0.43 (−41%)	*14.9 (28%)*	*66 (64%)*	*173 (8%)*
755	200	0.44 (−44%)	20.3 (44%)	78 (56%)	–
		0.46 (−43%)	*17.4 (33%)*	*60 (60%)*	*196 (7%)*
765	200	0.51 (−47%)	28.7 (54%)	271 (46%)	–
		0.53 (−46%)	*19.6 (34%)*	*72 (35%)*	*494 (31%)*
775	600	0.9 (−16%)	14.2 (−18%)	148 (−47%)	391 (100%)
785	600	1.0 (−4%)	16.7 (−9%)	132 (−87%)	212 (100%)
795	600	1.2 (−5%)	18.3 (−13%)	122 (−82%)	237 (100%)
810	600	1.0 (−4%)	18.7 (−12%)	125 (−86%)	207 (100%)
825	600	1.1* (−3%)	18.4* (−14%)	123* (−84%)	196 (100%)
Global fitting		0.2–1.1	18.4	79.3†; 123‡	208

*These lifetimes were fixed during the fitting (noisy curve).
†‡Parameters were determined for the kinetics measured at $\lambda_{det} \leq 765$ nm and $\lambda_{det} \geq 775$ nm, respectively. For further details, see text.

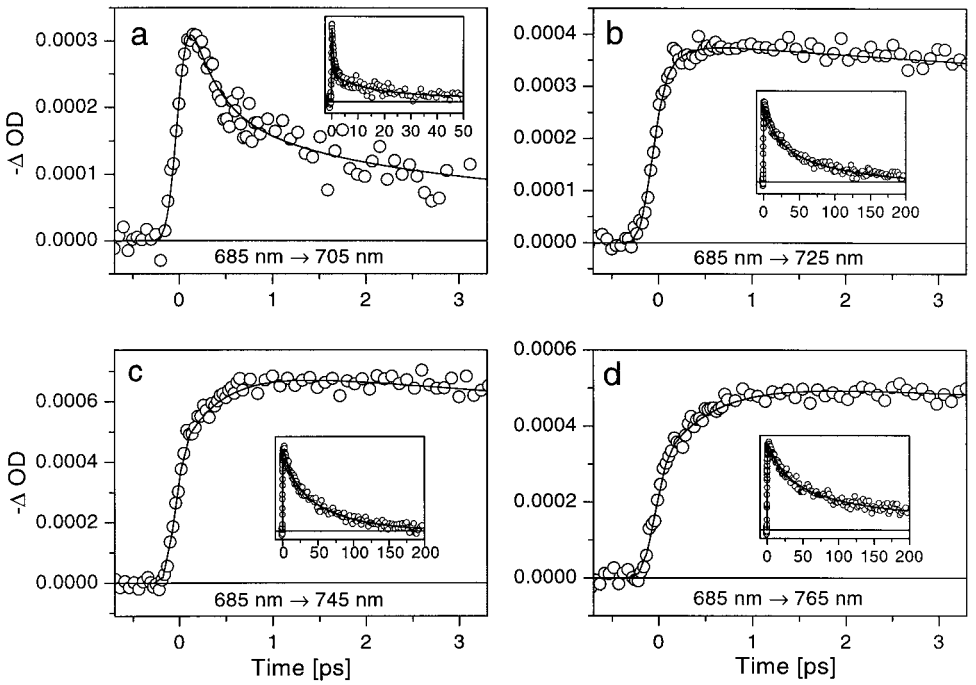

FIGUREE 3 The first 4 ps of the isotropic kinetics (*symbols*) probed at 705 nm (*a*), 725 nm (*b*), 745 nm (*c*), and 765 nm (*d*) upon excitation at 685 nm together with their fits (*lines*). The corresponding insets show the same kinetics in the extended timescale. Pump intensity was 1.4×10^{12} photons $\times$ cm^{-2} $\times$ pulse^{-1} (*a*) and 7×10^{11} photons $\times$ m^{-2} $\times$ pulse^{-1} (*b*, *c*, *d*). Sample OD was ~0.5 (*a*, *b*), ~1 (*c*), and ~3.5 (*d*) at the BChl *e* Q_y maximum.

It is noteworthy that the three-component fits lead to similar lifetimes (17–20 and 70–100 ps) at all wavelength through the BChl *e* region, with an exception for the kinetics measured at 705 nm, which is close to the isosbestic point. The lifetimes associated with the main decay components determined using the four-component fits appear slower with the increase of the probe wavelength. As shown in Table 1, the isotropic kinetics detected in the range of 725 nm $\leq \lambda_{det} \leq$ 755 nm are characterized by somewhat similar time constants (for a comparison of decays measured at the blue and red edges of the BChl *e* band, see Fig. 5 *a*), in contrast to those probed around 765 and 775 nm. In the latter case, both BChl *e* and BChl *a* contribute and those decays depend dramatically on the probe wavelength.

Rise in BChl *a*

As observed for BChl *e*, the isotropic kinetics measured within BChl *a* spectral region are also strongly pump-intensity dependent (Fig. 2 *b*); however, the effect becomes apparent at somewhat higher pump intensity (~1.5×10^{12} photons $\times$ pulse^{-1} $\times$ cm^{-2}). A dominant positive spike was

TABLE 2 An effect of excitation wavelength on kinetics measured for selected pump-probe wavelength combinations at low pump intensities: 4×10^{12} photons $\times$ pulse^{-1} $\times$ cm^{-2} for λ_{exc} = 505 nm (except for 3×10^{11} photons $\times$ pulse^{-1} $\times$ cm^{-2} for 505 nm→745 nm); 7×10^{11} photons $\times$ pulse^{-1} $\times$ cm^{-2} for λ_{exc} = 685 and 745 nm; and 3.5×10^{11} photons $\times$ pulse^{-1} $\times$ cm^{-2} for λ_{exc} = 715 nm

λ_{exc}- → λ_{det} (nm)	Scan length (ps)	τ_1 (ps) (A_1)	τ_2 (ps) (A_2)	τ_3(A_3) (ps)	τ_4(A_4) (ps)
505→715	100	0.91 (22%)	20.2 (34%)	78 (44%)	–
685→715	200	0.82 (26%)	17.2 (40%)	99 (34%)	–
		0.53 (12%)	*2.6 (25%)*	*28 (41%)*	*129 (22%)*
715→715	100	0.22 (19%)	2.8 (29%)	52 (52%)	–
		0.17 (25%)	*2.3 (15%)*	*11.8 (16%)*	*60 (40%)*
505→745	200	0.50 (−29%)	21.2 (35%)	82 (65%)	–
685→745	200	0.42 (−39%)	18.5 (37%)	82 (63%)	–
		0.43 (−41%)	*14.9 (28%)*	*66 (64%)*	*173 (8%)*
715→745	200	0.24 (−24%)	12.8 (26%)	67 (74%)	–
745→745	200	–	11.0 (41%)	66 (59%)	–
		2.3 (15%)	*15.9 (34%)*	*70 (51%)*	–
505→775	200	0.7 (−32%)	12.6 (−29%)	129 (−44%)	429 (100%)
685→775	600	0.9 (−16%)	14.2 (−18%)	148 (−47%)	391 (100%)
745→775*	600	0.04 (−14%)	15.2 (−5%)	151 (−81%)	259 (100%)
505→810	600	1.2 (−6%)	14.0 (−18%)	96 (−82%)	309 (100%)
685→810	600	1.0 (−4%)	18.7 (−12%)	125 (−86%)	207 (100%)
745→810	600	0.7 (−5%)	19.8 (−12%)	146 (−85%)	221 (100%)

*Kinetics could be fitted without subpicosecond component with the same χ^2.

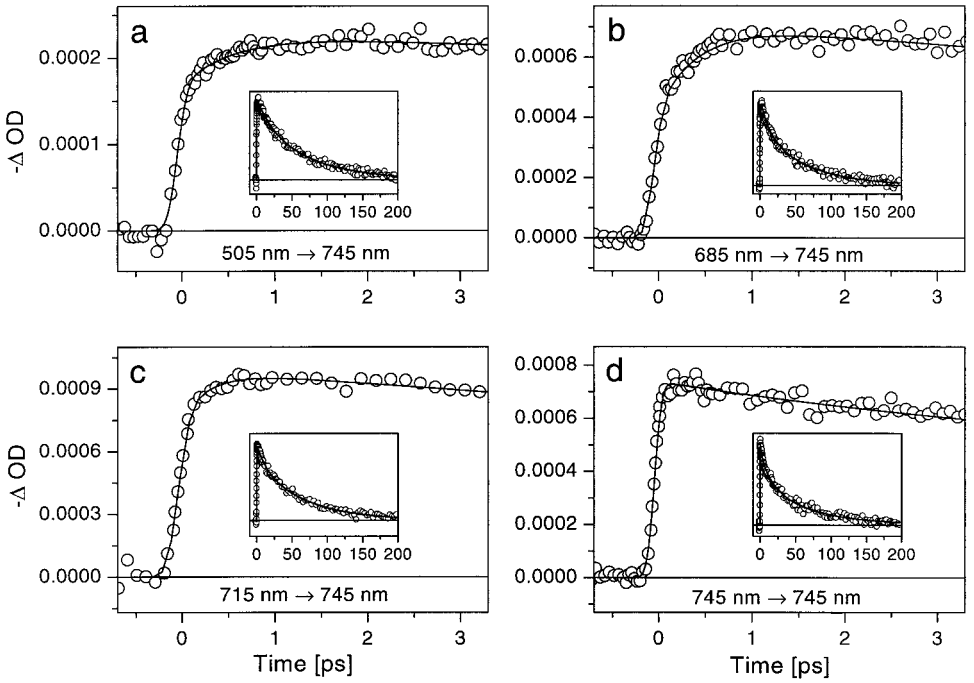

FIGURE 4 The first 4 ps of the isotropic kinetics (*symbols*) probed at 745 nm upon excitation at 505 nm (*a*), 685 nm (*b*), 715 nm (*c*), and 745 nm (*d*) together with their fits (*lines*). Insets show the same data on extended timescale. Pump intensity was 3×10^{11} photons $\times$ cm^{-2} $\times$ pulse^{-1} (*a*), 7×10^{11} photons $\times$ cm^{-2} $\times$ pulse^{-1} (*b*, *d*), and 3.5×10^{11} photons $\times$ cm^{-2} $\times$ pulse^{-1} (*c*). Sample OD was ~1 at the BChl *e* Q_y maximum.

observed at higher intensities, which is significantly attenuated at lower pump intensities. Under the annihilation-free conditions and at wavelengths below 800 nm, this spike almost disappears and instead a minor rise component with a lifetime ~1 ps appears (inset of Fig. 2 *b*). A similar lifetime can also fit the remaining spike seen at $\lambda_{det} > 800$ nm (Table 1; Fig. 5 *b*). Except the initial part and the overall amplitude, the kinetics measured at all probe wavelengths within BChl *a* region ($\lambda_{det} > 775$ nm) are very similar, showing negligible dependence on the detection wavelength (Fig. 5 *b*). The change of the pump wavelength has also only moderate effect on the kinetics, and this time shows an opposite trend in comparison to the decay BChl *e*: the resolved rise times at a given probe wavelength are faster with a shorter pump wavelength. The profiles are dominated by a slow rise, which requires two exponential components for satisfactory fits. Attempt to fit the kinetics with a single rise component leads to a lifetime of ~70–80 ps, but the fits exhibit a remarkable deviation from experimental data. The faster rise component with an amplitude of 10–14% has a very similar lifetime (~17–19 ps) as the faster component of the BChl *e* decay, obtained from the three-component fits. The slower and also the dominant rise component is characterized by a lifetime of 120–130 ps, which is considerably slower than the 70–100 ps decay component of BChl *e*. This slower rise is in fact rather close to the slowest lifetime resolved from the kinetics detected around the BChl *e* absorption maximum using four exponential components. The subsequent BChl *a* decay was characterized by a lifetime of ~200–240 ps for kinetics excited at $\lambda_{exc} \geq 685$ nm.

Global lifetime analysis

The similarity between the lifetimes resolved using the three-component fitting within BChl *e* region, together with the similar lifetimes resolved from the kinetics probed within BChl *a*, justify the use of global lifetime analysis. This analysis enables the determination of the fitting parameters with a higher accuracy than from the single decay fit.

The global analysis was applied to the kinetics measured upon excitation at 685 nm. The first model function consists of three and four exponential components for the kinetics probed in the BChl *e* and *a* regions, respectively, in which one component (τ_1) and its amplitude were held as local free parameters. This enabled reasonably fitting of the initial part of the kinetics at all wavelengths, including the one at 705 nm, where τ_1 was obtained to be 0.74 ps. At other wavelengths, the fitting of the initial part gives a lifetime and an amplitude that are always in good agreement with the parameters obtained from the corresponding single decay fits (Table 1). The best fits and the smallest weighted χ^2 were obtained when different τ_3 lifetimes (see Table 1) are assumed for the kinetics measured in BChl *e* and BChl *a* spectral region. In fact, this difference is expected on closer inspection of the parameters determined from the corresponding single decay fits. The lifetimes obtained from the global analysis are 18.4 ps (τ_2), 79.3 ps (τ_3) for the kinetics probed within BChl *e*, and 18.4 ps (τ_2), 123 ps (τ_3) and 208 ps (τ_4) for those measured in BChl *a* region. The corresponding amplitudes are plotted as decay associated spectra (DAS) in Fig. 6.

For comparison, the global analysis was also performed with four components. Although the lifetime and amplitude

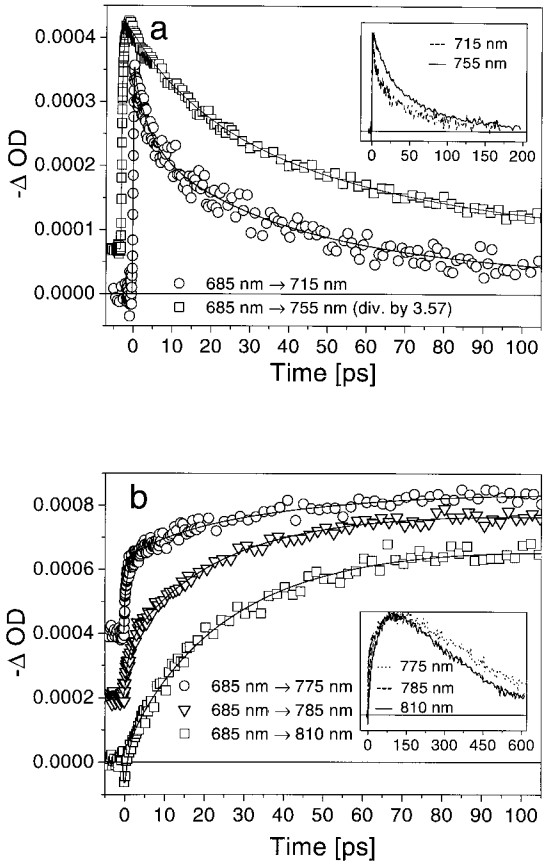

FIGURE 5 Isotropic kinetics measured within BChl *e* (*a*) at 715 (○) and 755 nm (□, divided by 3.57 for the sake of comparison) and in the BChl *a* region (*b*) at 775 nm (○), 785 nm (▽), and 810 nm (□) together with their fits. Kinetics are offset respectively for clarity. Insets show the same data after normalization at the maximal amplitudes and on extended timescale. The pump wavelength is 685 nm, pump intensity was 7×10^{11} photons $\times$ $cm^{-2} \times pulse^{-1}$; sample OD was 3.5 at the BChl *e* Q_y maximum, except for (*a*, ○) where it was 0.5.

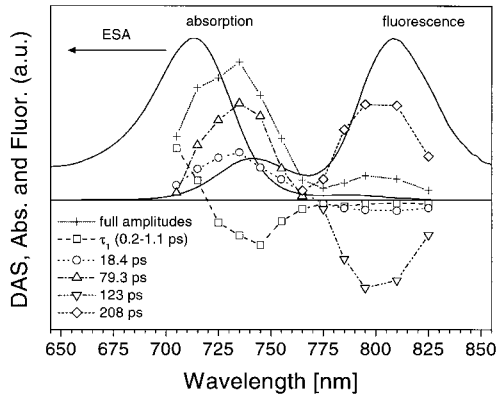

FIGURE 6 Decay associated spectra obtained from global lifetime analysis of the isotropic kinetics upon excitation at 685 nm. The steady-state absorption and fluorescence spectra are also shown.

associated with the fastest component were kept again as local parameters, we released the restrictions applied in the previous case and all three remaining components were considered as truly global ones within the whole spectral range. As a consequence, the time constants of the decay and rise terms in BChl *e* and BChl *a*, respectively, were forced to be identical. This analysis gives lifetimes of 20.7 ps (τ_2), 102.3 ps (τ_3), and 211 ps (τ_4) for the global parameters. The corresponding DAS (not shown) was very similar to that obtained in the previous case, except that the DAS of 79.3 and 123 ps were replaced by the one with lifetime of the 102.3 ps, and the relative amplitudes of 20.7 and 102.3 ps components were almost the same (~50%) in BChl *e* spectral region. In addition, the 212 ps component has a negligible amplitude for $\lambda_{det} < 765$ nm. The weighted χ^2 (1.1) for this analysis was worse than that obtained in the previous case (1.05)

The DAS provide a straightforward visualization of the excitation relaxation processes within the chlorosome. The rise observed within first 1 ps in the BChl *e* region is connected with a relaxation from some high-energy excited states to the states from which eventual emission occurs. On closer inspection of Fig. 6, one will find that the DAS of the 0.2–1.1 ps component is nearly a perfect mirror image of the BChl *e* fluorescence spectrum, both having maxima around 745 nm. Energy transfer from BChl *e* to BChl *a* occurs in two main steps: first ~15% of the energy is transferred in 18–21 ps, and the main portion of energy arrives with a substantial delay. The results obtained from the single decay fitting and from the first global analysis (Fig. 6) suggest that the time constants associated with the second step are different for the decay of BChl *e* and the rise of BChl *a*. If these two time constants are forced to be identical, a lifetime of ~100 ps is obtained. The subsequent decay of BChl *a* occurred with a ~200 ps lifetime.

Anisotropy decays

Additional information about the excitation relaxation processes within the chlorosome was obtained from the anisotropy decays. Similarly as for the isotropic decays, the anisotropic decays are also strongly pump-intensity dependent (Table 3; Fig. 7). Besides obviously faster decay, the increase of pump intensity further leads to a lower value of residual anisotropy. Under the annihilation-free condition, the anisotropy decays measured within the BChl *e* region are rather slow, and this decay can be fairly well fitted by a single exponential component with a lifetime between 10–20 ps (Fig. 8). The parameters characterizing the anisotropy decay are quite well reproducible considering the low pump intensities used. For instance, independent measurements for 685→745 nm pump-probe combination give lifetimes between 13.5–17.5 ps, initial anisotropy from 0.26 to 0.30, and the residual anisotropy always 0.16. Addition of the second decay component does not lead to any improvement of the fit. The lifetime also depends on pump-probe wavelength separation in a similar way like the isotropic

TABLE 3 Comparison of pump intensity dependence for the fitting parameters determined in the isotropic and anisotropy decays excited at 715 nm and probed at 745 nm

I_{exc} (photons × pulse^{-1} × cm^{-2})	τ_1 (A_1) (ps)	τ_2 (A_2) (ps)	τ_3(A_3) (ps)	τ_{anis} (ps)	$r(0)$	$r(\infty)$
3.5×10^{11}	0.24 (−24%)	12.8 (26%)	67 (74%)	13.3	0.32	0.19
7.0×10^{11}	0.20 (−21%)	10.2 (42%)	58 (58%)	10.6	0.30	0.16
3.5×10^{12}	0.15 (−6%)	5.3 (55%)	36 (45%)	6.2	0.31	0.14
1.4×10^{13}	–	2.6 (72%)	30 (28%)	2.6	0.28	0.06

decays. However, the difference of $r(0) - r(\infty)$ is similar for different pump-probe wavelength combinations at low pump intensities, and values between 0.12–0.15 were found (Fig. 8). For the decays measured in the red part of the BChl *e* absorption band (Figs. 7 and 8), the initial anisotropy values were found to be significantly less than 0.4, indicating nonzero angle between transition dipole moments at the pump and probe wavelengths. Only in these cases do the residual values differ considerably from steady-state fluorescence anisotropy, 0.24, determined previously (Arellano et al., 2000).

For a given pump-probe wavelength combination, the lifetime of the anisotropy decay probed in the BChl *e* region is fairly close to the 10–20 ps decay component of the corresponding isotropic kinetics. This correspondence holds true even at higher pump intensities as long as anisotropy decays are fitted with a single exponential, although use of a second faster component gives somewhat better fit to the calculated anisotropy decays in this case (data not shown). Under even higher intensities, the anisotropy decay appears no longer monotonic, as observed also for the isotropic decays. For instance, under a pump intensity of 7×10^{13} photons × pulse^{-1} × cm^{-2}, the anisotropy obtained at 745 nm upon excitation at 715 nm reaches a minimum of −0.6 in the first 10 ps and then rises again up to 0.05 (not shown).

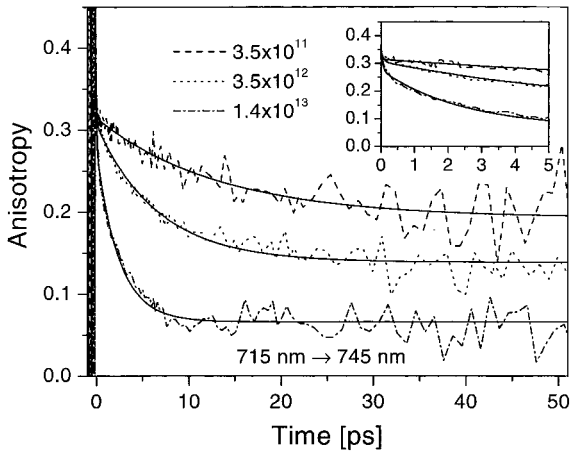

FIGURE 7 Pump-intensity dependence of the anisotropy decays probed at 745 nm upon excitation at 715 nm together with the corresponding single exponential fits. Insets show the first 5 ps of the same data. Intensities are in photons × cm^{-2} × pulse^{-1}, and the sample OD ~1 at the BChl *e* Q_y maximum. The decay time, initial, and residual anisotropies are listed in Table 3.

Anisotropy decays in the BChl *a* region were measured at 795 nm upon excitation at 685 nm. Both the parallel and perpendicular polarized kinetics are of similar shape, and the amplitude of the perpendicular one is slightly larger than the parallel one (not shown). As a result, the calculated anisotropy decays are rather noisy, so their lifetimes and especially the initial anisotropies are determined with a relatively large uncertainty. Nevertheless, the decay is obviously much faster than the decay obtained for BChl *e*. Best fits were obtained with a lifetime of 0.9–1.4 ps and initial values of 0.2 ± 0.07, which is in the same range as the residual values found for BChl *e*, 0.15–0.25. The residual anisotropy of BChl *a* was ~(−0.09)–(−0.1), in good agreement with the steady-state values (Arellano et al., 2000).

MODELING OF OPTICAL SPECTRA

Our interpretation of the experimental data is based on the structural model for the bacteriochlorophyllide *d* aggregate, proposed according to the quantum and molecular modeling calculations (Holzwarth and Schaffner, 1994). Slightly different structural parameters were reported for BChl *c* (Prokhorenko et al., 2000). These models accommodate the bonds that are responsible for vibrations observed in Raman and infrared spectroscopy (Hildebrandt et al., 1991; Chiefari et al., 1995) and the intermolecular cross correlations observed in magic-angle spinning NMR spectroscopy (Balaban et al., 1995, Boender et al., 1995). The latter method was recently used to refine the model (van Rossum et al., 2001). Assembly of BChl molecules in these structures is also in agreement with optically detected magnetic resonance data (Psencik et al., 1997). Even if the model still cannot be regarded as definitive, it represents a solid base for testing the optical properties of aggregates. The aggregates are characterized by strong pigment-pigment interactions between the BChls, and, in addition, there is very little amount of protein in chlorosomes, which means a minimal disturbance from pigment-protein interaction. These features make the chlorosomes ideally suited for the application of exciton theory (Lin et al., 1991; Alden et al., 1992; Buck and Struve, 1996; Somsen et al., 1996; Arellano et al., 2000; Prokhorenko et al., 2000).

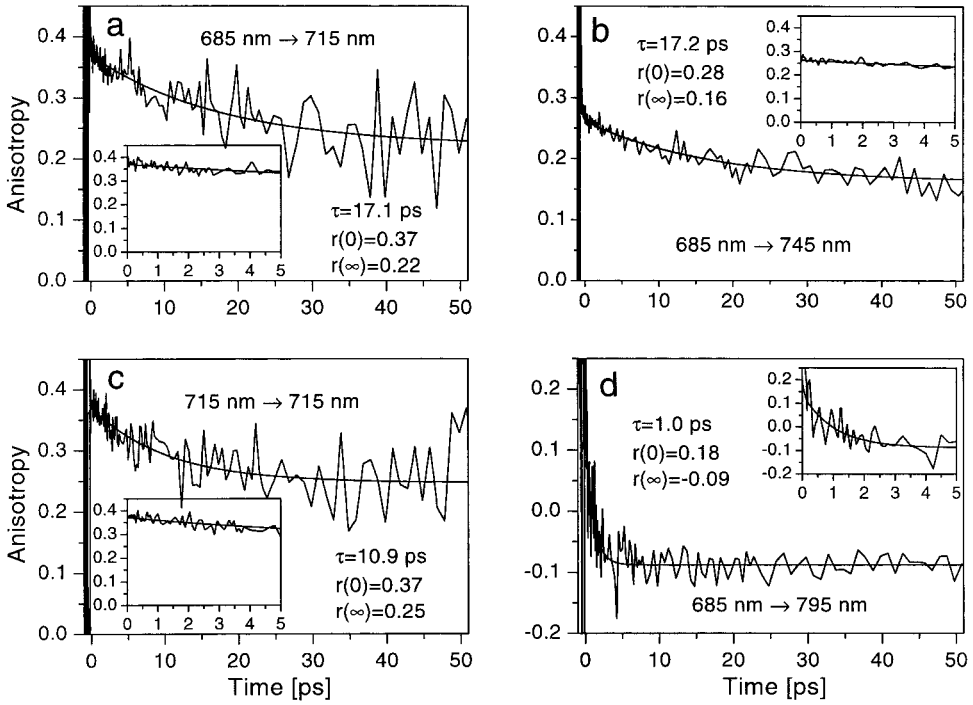

FIGURE 8 Anisotropy decays obtained for different pump-probe wavelength combinations as indicated, together with the corresponding fits. Insets show the first 5 ps of the anisotropy decay. The decay time, initial, and residual anisotropies are also shown. Pump intensity was 1.4×10^{12} photons $\times$ cm^{-2} $\times$ pulse^{-1} (*a*, *d*), 7×10^{11} photons $\times$ cm^{-2} $\times$ pulse^{-1} (*b*), and 3.5×10^{11} photons $\times$ cm^{-2} $\times$ pulse^{-1} (*c*). Sample OD was 0.25 (*a*, *c*) and 1 (*b*, *d*).

Optical spectra were calculated in the point-dipole approximation as described in the Appendix. If the macrocycles of the pigments are in or close to van der Waals contact, such as the BChls in the chlorosomes, the point-dipole approximation is no longer valid and more realistic description of charge density is necessary. However, it often turns out in practice that point dipoles work well even for closer approaches (Pearlstein, 1991). Although the use of extended transition-charge distributions certainly can affect the calculated values of exciton interaction energies, they have no effect on the forms of the expressions for spectra calculations (Pearlstein, 1991). In addition to chlorosomes (see above), point-dipole approximation was successfully used for numerous coupled pigment complexes of various photosynthetic organisms (for a recent review, see van Amerongen et al., 2000).

For comparison, absorption and circular dichroism (CD) spectra were calculated using the parameters given by Prokhorenko et al. (2000), and essentially identical results were obtained as those presented therein (not shown). The only difference is the opposite sign of the CD signal, indicating opposite chirality of the aggregate (mirror image). One common result of these comparative calculations is worth mentioning here: the two exciton states possessing almost all the oscillator strength are located within 100 cm^{-1} from the lowest exciton state for the two structures (without inclusion of the disorder) presented by Prokhorenko et al. (2000).

As there is no structural model available for BChl *e* aggregates, we use those parameters of the original model with small changes. Our major modification to the model is an alteration of the angle between the direction of the Q_y transition dipole moment of BChl molecule and the *z* axis of the rod, denoted here by γ. From fluorescence anisotropy data measured for *Cb. phaeobacteroides*, it was calculated that $\gamma = 19$–$23°$ depending on the extent of the initial delocalization (Arellano et al., 2000). These γ values are in overall good agreement with previous results of linear dichroism (LD) in gels and in electric fields, polarized fluorescence on random samples, and on ordered samples and ps pump-probe experiments, which give values between 15 and 25° for *Cf. aurantiacus* (van Amerongen et al., 1988; Griebenow et al., 1991; van Amerongen et al., 1991; Ma et al., 1996; Frese et al., 1997). Values out of this range reported include the measurements performed by van Dorrsen et al. (1986) and by Fetisova et al. (1986) on the chlorosomes from *Cf. aurantiacus* and *Cb. limicola*, respectively, giving an angle of 37° and 0°. The former is identical to the angle of 36.7° determined for the original model (Prokhorenko et al., 2000). However, it was shown by van Amerongen et al. (1988) that this angle is too large, probably due to an overestimation of the extent of ordering of the chlorosomes. It should be noted that the values obtained from LD reflect the (weighted) average of the transition dipole moment orientation of the states absorbing at the given wavelength with respect to the rod axis. In contrast, the values determined by means of fluorescence anisotropy are given by the average angle between transition dipole moments of the absorbing and emitting states, which for excitation near the absorption maximum and detection in the red part of the absorption band should be close to γ (see Discussion).

In this work, we intend to show that the optical spectra calculated using the γ value of 20° (calculated from the steady-state anisotropy data) show better agreement with some experimental data. The remaining structural parameters were recalculated in such a way that the distances given by hydrogen bond network are kept the same as those given in the original model (Holzwarth and Schaffner, 1994, Prokhorenko et al., 2000). Furthermore, the main features of the model were conserved, namely an organization of the BChl molecules into linear stacks parallel to the symmetry axis of the aggregate and additional helical hydrogen bond network (Fig. 9). The recalculation led to a smaller distance between the centers of the stacks (0.46 nm instead of 0.8 nm), a larger distance between the molecules within the stack (0.83 nm instead of 0.65 nm, measured in term of Mg-Mg distance), as well as a larger angle of hydrogen-to-keto oxygen hydrogen bond (~170° instead of 139–153°) with respect to the original model (Holzwarth and Schaffner, 1994, Prokhorenko et al., 2000). As a result, the number of stacks per 360° increases from 36 to 62 for the rod with the same diameter, and the overall number of pigments per unit length of the rod increases 1.25 times compared to the original model. It should be noted that similar results to those presented here could be obtained with an alternative model with the same density of pigments as in the original model, providing the distance between the planes was increased and dielectric constant of 1.00 was used. However, neither quantum calculations and molecular modeling (which have not been done for BChl *e* so far) nor experimental data supports such a model.

The structural parameters used in this work are slightly different from those used by Arellano et al. (2000), where exciton calculation was applied to simulate the effect of the angle γ change on absorption and CD spectra. The angle of hydrogen-to-keto oxygen hydrogen bond was treated as an additional variable, whereas it was kept 180° previously. In addition, we selected differently the 15 × 15 aggregate for our calculation. We believe that these changes provide better correspondence to the original model. However, because these changes give rise to only very moderate changes in calculated spectra, they do not affect the conclusions presented in our previous work (Arellano et al., 2000).

Fig. 10 *a* shows the stick spectra calculated for 15 × 15 and 62 × 20 nondisordered aggregates. The latter represents a close tubular structure. A comparison between the calculation results shows that for the 15 × 15 aggregate the basic spectral features are already well established. Fig. 10 *a* also shows the envelope of the stick spectrum convoluted with a Gaussian function, and for illustration only, one CD spectrum is shown. The calculated absorption maximum is ~380–400 cm^{-1} blue shifted from the respective lowest exciton level located at 735–740 nm for both 15 × 15 and 62 × 20 aggregates. This shift is more than four times larger compared to that calculated using the parameters of the original model (~60–90 cm^{-1}), either for the 18 × 8 or the

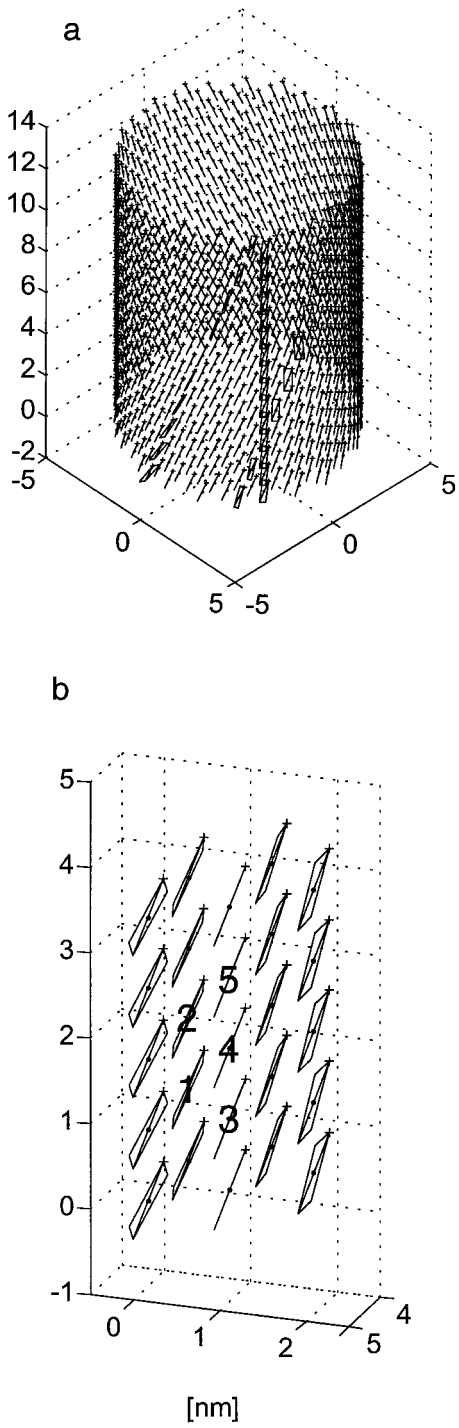

FIGURE 9 Model of a point-dipole distribution used for the spectra calculations. Panorama view of the 62 × 15 aggregate (*a*) and a detailed view of the 5 × 5 aggregate (*b*). Position of the dipoles are denoted by dots and their orientation by a line ended with symbol +. The length of the line roughly corresponds to the diameter of the porphyrin ring. Some planes of BChl molecules are schematically drawn, assuming for simplicity that the Q_y transition dipole moment is parallel to the *y* axis of the porphyrin ring. All distances are in nanometers, structural parameters in Table 4.

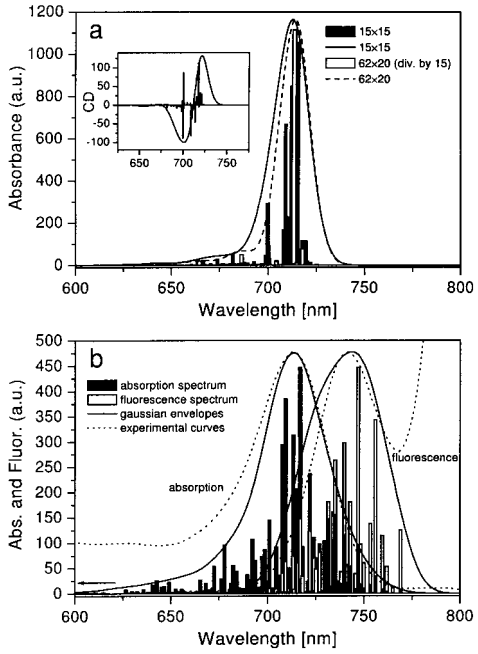

FIGURE 10 (*a*) Calculated absorption stick spectra for perfect aggregates consisting of 15 × 15 and 62 × 20 molecules, together with the sum of their Gaussian envelopes. Each of the envelopes has a FWHM of 350 cm^{-1} (Prokhorenko et al., 2000). The inset shows the calculated CD spectrum for the 15 × 15 aggregate. (*b*) Gaussian envelope of absorption and fluorescence spectra for the 15 × 15 aggregate obtained by averaging 5000 different realizations of the diagonal disorder, which is assumed to have normal distribution with standard deviation of 415 cm^{-1}. For comparison, the absorption and fluorescence stick spectra obtained for one particular realization of the disorder are also shown. The fluorescence components were calculated for the temperature of 300 K and were normalized to the maximal absorption component. Absorbance of monomer corresponds to 23 units (BChl *e* dipole strength in $Debye^2$) in the arbitrary scale used and is indicated by an arrow. The dielectric constant used both in (*a*) and (*b*) is 1.05, and all other parameters are given in the Appendix. The dotted lines are experimental curves measured at room temperature.

36 × 8 aggregate (Prokhorenko et al., 2000). However, as the lower levels possess almost no oscillator strength, the calculated fluorescence spectrum exhibits only a slightly enhanced Stokes shift compared to the original model (not shown). In addition, the higher-lying exciton states located above 650 nm also carry negligible oscillator strengths.

Due to expected random fluctuations of the molecular energies, the aggregate cannot be regarded as perfect and an effect of energetic disorder has to be included to get realistic spectra. To fit the experimental absorption and fluorescence spectra, a normal distribution of site energies (Δ_i in Eq. 3) with standard deviation of ~400 cm^{-1} was used. Inclusion of the diagonal disorder leads to broadening of the spectrum and, more importantly, to redistribution of the oscillator strength from the highly allowed transitions mainly to those in the red part of the absorption spectrum (Fig. 10 *b*). Nevertheless, the lowest states still posses small oscillator strength. Fig. 10 *b* also shows the Gaussian envelope of absorption spectrum averaged over 5000 different realizations of the disorder (standard deviation of 415 cm^{-1}) for the 15 × 15 aggregate. Among the overall 225 exciton states for each realization of the disorder, there are typically 100 states having negligible dipole strength (less than 0.1 of the monomer value), another 80 states have their dipole strength between 0.1 and 1 of the monomer value, ~40 states fit between 1–10 of the monomer value, and around five states posses a dipole strength that is more than 10 times higher than that of the monomer. The distribution of the 5000 lowest exciton levels is characterized by a distribution function with a maximum at 765 nm and FWHM of 220 cm^{-1} (not shown). Individual lowest exciton levels are characterized by a transition dipole strength ranging from <1% to 300% (mean value ~90%) of the monomer BChl *e* dipole strength. The width of the distribution function of the lowest exciton levels fits well with that determined by hole burning in fluorescence spectra of *Cb. tepidum* (Psencik et al., 1998), where it was shown that this distribution function corresponds to the overall emission spectrum of aggregated BChl at 4.2 K (FWHM of ~250 cm^{-1}).

The calculated spectrum retains well the main features of the experimental spectrum: 1), a large red shift of the absorption maximum (~715 nm) compared to that of the monomer (~660 nm); 2), asymmetry of the band with an enhanced absorption on the blue side together with the shoulder at ~675 nm; and 3), transitions to the higher exciton states possess the dominant oscillator strength as predicted by hole-burning data (Fetisova and Mauring, 1992, Psencik et al., 1998 and references therein). Moreover, the same parameters used to obtain the absorption spectrum that is in the best agreement with the experimental data also give rise to the best results for calculated room temperature fluorescence spectrum in terms of its maximum (~745 nm), Stokes shift, and the width of the band (Fig. 10 *b*). This calculation shows that use of an angle $\gamma = 20°$, determined experimentally, is capable of reproducing the absorption and CD spectra and, in contrast to the original model, the unusually large red shift of the fluorescence emission spectra. Further, it is unnecessary to take into account other interactions, such as the coupling between the aggregates (rods), to get realistic spectra. Therefore this calculation may also be applied to simulate the spectra of (individual) aggregates formed spontaneously in solutions.

With the parameters used by Prokhorenko et al. (2000), the strongest coupling is between the monomer 1 and 2 within the same stack (Table 4; Fig. 9 *b*). In our modified model, the situation is more complicated, as the modification of γ changes the mutual orientation of the interacting dipoles, which in turn affects the exciton couplings. The strongest interactions are between dipoles 1 and 3 as well as 1 and 4; both of them have similar energy but opposite signs. Nevertheless, the negative coupling energies, which arise from the head-to-tail interaction between the dipoles (typical for J-aggregates) play a dominant role in the aggregate,

TABLE 4 Interaction and structural parameters for pairs of dipoles

Pair of dipoles	σ (°)	r (nm)	V (cm^{-1})	κ^2	κ^2/r^6 (nm^{-6})
		original model*			
1-2	0	0.65	−513	0.87	11.54
1-3	6	1.03	+137	0.97	0.81
1-4	6	0.80	−17	0.01	0.04
1-5	6	1.03	−248	3.24	2.71
		modified model			
1-2	0	0.83	−335	2.71	8.29
1-3	2	0.55	+562	0.68	24.57
1-4	2	0.69	−555	2.54	23.54
1-5	2	1.43	−80	3.98	0.47

See Fig. 9 *b* for labeling and Appendix for the definition of the parameters; dielectric constant of 1.0 was used. σ is the angle between the two dipoles. *Parameters were calculated on the basis of structural parameters given by Prokhorenko et al. (2000).

similarly as in the original model. This is clearly demonstrated by the pronounced red shift (more than 1000 cm^{-1}) of the calculated absorption maximum with respect to that of monomeric BChl *e*, in agreement with experimental data. Moreover, the interaction in parallel fashion (typical for H-aggregates) is enhanced in our model. That results in a substantial energy difference between transitions with the largest oscillator strength and the lowest-lying exciton levels. This difference leads to a >500 cm^{-1} Stokes shift, which is also observed experimentally, owing to Boltzmann population distribution between these states.

Recently a refined model including a bilayer structure for the aggregates of *Cb. tepidum* was published (van Rossum et al., 2001); however, exciton calculation based on this model has not been reported yet.

As noticed, the choice of smaller γ (20°), compared to 36.7° used in the original model, is based merely on results of various experimental techniques utilizing polarized light. However, we believe that the good agreement between the model calculations and experimental data justifies the use of this modified model as a working hypothesis, which should be either proved or rejected by further work. The question remaining to be justified is if the proposed changes are consistent with the NMR data (Rossum et al., 2001 and the references therein). Also we believe that it is important to consider the possible distortion of the structure by other molecules, such as carotenoids (Ma et al., 1996; Arellano et al., 2000), which has not been well defined yet. It should be emphasized, however, that the main conclusions of this work are also valid within the original model, unless mentioned specifically in the text.

DISCUSSION

The densely packed pigments in chlorosomes and the rapid energy transfer between them lead to onset of exciton annihilation at remarkably low light level. However, this process is unlikely to operate at physiological conditions because of the low light available. Considering the excitation intensities used in this work to obtain annihilation-free kinetics (2–7 × 10^{11} photons × pulse^{-1} × cm^{-2}), one will find that they are strikingly different from the light-harvesting complexes of purple bacteria, where annihilation is usually observable at an intensity that is ~2 orders of magnitude higher (Ma et al., 1997). Actually, the applied pump intensities correspond to only a few photons per chlorosome, each consisting presumably of ~10^5 molecules. To reveal the actual energy transfer dynamics in the chlorosomes, it is crucial to perform all the measurements under very low pump intensities, and to extract kinetic information from annihilation-free kinetics. Due to this consideration, we will not discuss the kinetics dominated by ESA ($\lambda_{det} \leq 700$ nm) in the rest of the paper, for which it was difficult to eliminate the annihilation effect.

Early energy transfer processes within BChl *e*

Under the low excitation intensities, we observed for the first time a subpicosecond relaxation process within the chlorosome BChl aggregates at room temperature, which is manifested by a rise in the kinetics probed in the red part of the Q_y absorption band of the BChl *e*. The rise component has a decay counterpart in the kinetics probed at wavelengths shorter than 725 nm. However, at least part of this decay might be an artifact inasmuch as the probe wavelength is close to the isosbestic point at ~700 nm. The lifetime (~0.2–0.5 ps) and amplitude associated with the rise were found to increase with the spectral separation between pump and probe wavelengths within the BChl *e* Q_y band. When excited at 505 nm, two additional processes contribute to the rise observed in the BChl *e* Q_y band apart from the relaxation within the Q_y manifold itself: a <100 fs energy transfer from the carotenoid S_2 state (Psencik et al., 2002) and the internal conversion from the Soret-to-Q_y band. The latter is also expected to occur with a <100 fs lifetime (Psencik et al., 2002). However, the rise observed upon 505 nm excitation is characterized by a smaller amplitude, and the rise time at 745 nm is only by ~80 fs slower compared to those resolved upon excitation at 685 nm. These results can be explained by a nonselective population of all the states within the Q_y manifold through the internal conversion from the Soret-to-Q_y band. Subsequent relaxation within the Q_y band can be described as a weighted average of relaxation from all the states located between the blue edge of the band and 745 nm. The idea is supported by the fact that excitation at 715 nm, where the density of states is the highest, leads to a significantly faster rise with a smaller amplitude at 745 nm compared to the excitation at 685 nm (Table 2).

By comparing the DAS of the rise component with steady-state absorption and emission of BChl *e* (Fig. 6), it can be clearly seen that the rise is due to relaxation and/or energy transfer from the higher energy excited states to the lower

energy states, which give rise to fluorescence. The process is rather fast: for instance, the relaxation from the states absorbing at 685 nm to those at 745 nm with an energy difference of $\sim$1200 cm^{-1} occurs with a lifetime less than 0.5 ps. It suggests that the rise may be due to an exciton relaxation rather than stepwise Förster hopping of localized excitations, which would involve many transfer steps owing to the huge number of molecules in the chlorosome. This attribution is supported by following considerations: 1), Strong exciton coupling between the BChl *e* molecules leads to energy level splitting (Fig. 10 for our model), and the relaxation between the exciton levels is induced by electron-phonon coupling. In the presence of disorder, the relaxation is connected with a spatial redistribution of the energy as the excitation is not perfectly delocalized. 2), The rise was observed for certain pump–probe wavelength combinations, such as 715 nm→745 nm but not for 685 nm→715 nm, although their energy difference is similar. However, only in the former case the low-energy and presumably longer-lived exciton states are probed. 3), Low temperature hole burning showed that zero phonon holes can be burned only in the red edge of the aggregated BChl Q_y absorption band. This is explained by a longer lifetime of the lower exciton levels, where the energy is accumulated after fast exciton relaxation and/or energy transfer (Fetisova and Mauring, 1992; Psencik et al., 1998 and references therein). Also it is unlikely that the process is due to a vibrational relaxation, inasmuch as $Q_y(0,0)$ band was most probably both excited and probed in the experiments with excitation at 685 nm.

Another important observation at low pump intensity is the minor depolarization within the first 1 ps in the BChl *e* region and no need for a subpicosecond component to fit the data. Instead, the anisotropy decay is remarkably slow (10–20 ps) compared to previously reported data (300 fs–1.5 ps, Savikhin et al., 1994; 1.7–3.7 ps, Savikhin et al.; 1995; 4–7 ps, Lin et al., 1991). This is in contrast to the situation in the exciton coupled B850 ring of purple bacteria, where the depolarization is completed within few hundreds of femtoseconds (e.g., Bradforth et al., 1995; Ma et al., 1997, 1998). In the B850, both the transition dipoles of individual molecules and the main exciton transitions are oriented nearly parallel to the ring plane. Calculations based on our model aggregate show that for both perfect and disordered aggregates, most of the exciton transitions carrying significant oscillator strength orient in close to parallel with respect to each other and to the symmetry axis *z*, provided that a fragment representing closed tubular structure is considered. Relaxation between these states, which are responsible for the major part of the TA signal in an isotropic decay, would not induce a significant anisotropy change. This explains well the presence of the fast decay or rise only in the isotropic kinetics, but not in the corresponding anisotropic profiles.

From the above discussion, it follows that within our model it is impossible to attribute the anisotropy decay to the exciton relaxation between the main absorbing exciton levels belonging to closed tubular structure. To explain the experimentally observed anisotropy decays, we need to consider the states with different orientations. Our calculations show that in the presence of disorder there are many states possessing small but not negligible oscillator strengths (comparable to that of the monomer) and having a localized character. In addition, the transition moments associated with these states orient often in such a way that are close to the transition moments of the individual molecules, at which position the amplitude of the corresponding exciton state wave function is dominant. The portion of the states with small oscillator strengths increases toward the edges of the absorption band. Relaxation and/or energy transfer between these states will lead to the observed anisotropy decay, even at 715 nm, where the main transitions are presumably parallel to the chlorosome axis. Such a behavior seems to be in agreement with the results of calculations for the exciton coupled B850 ring, where the presence of energetic disorder brings the most localized character to those exciton states at the edges of the absorption band, whereas the extent of delocalization is maximal in the middle of the band (Pullerits, 2000).

Experimental support for the prevailing localization of the long-wavelength absorbing BChl *e* states is given by the initial anisotropies. The initial anisotropy was found to be significantly lower than 0.4, when probe wavelength is tuned into the SE band, e.g., to 745 nm (Fig. 7 and Fig. 8 *b*). For the 715→745 nm pump-probe combination, the initial anisotropy was found to be 0.32. The pump wavelength corresponds to the absorption maximum in this case, where all the main absorbing transition dipoles were calculated to be nearly parallel to the rod axis even in a presence of a diagonal disorder. In accordance with the previous discussion, we further assume that the states with small oscillator strengths probed at 745 nm have, on average, orientation of their dipole moments close to that of individual molecules. In this case, the angle between excited and probed transitions will be close to 20° in our model, giving an initial anisotropy of 0.33, which is close to the observed value. For other pump-probe wavelength combinations, determination of the angle between excited and probed transition is complicated by the mixed contribution of differently oriented transition dipoles at both pump and probe wavelengths. However, the results seem to be in agreement with exciton calculations of Lin et al. (1991), showing that the blue exciton bands have different dipole orientations in comparison to those of the main band. Despite the experimental uncertainty in the initial anisotropy determination and simplification in the calculation of $r(0)$, the above discussion indicates that after fast initial exciton relaxation, the excitation will be found in rather localized states. When excitation gets localized, the subsequent transfer around the rod would lead to the decay of anisotropy, inasmuch as transition moments of individual

molecules are parallel within the stack, but there is a nonzero angle between the dipoles from different stacks.

The states with localized character would not be necessary to explain the anisotropy decay if only a part of the aggregate is considered, like one stack, the 5×5 one shown in Fig. 9 *b* or the 15×15 aggregates used for the calculation of the optical spectra. In this case, the main exciton transitions have their orientation close to that of individual molecules, even without inclusion of disorder. If the chlorosome is formed by such aggregates that are weakly coupled together, it would be again only energy transfer around curvature of the whole oligomer that could lead to the anisotropy decay (e.g., excitation transfer to the neighboring stack or aggregate, respectively).

In either case, we propose that the 10–20 ps anisotropy decays observed within BChl *e* region are related to the redistribution of excitation energy around the circumference of the rod, leading to energy equilibrium around the entire rod. The process occurs most probably between the more localized states, populated as the result of exciton relaxation. If this attribution is correct, then the ~15 ps lifetimes observed in this work are in agreement with the 7-ps anisotropy decay observed for *Cf. aurantiacus* chlorosomes by Lin et al (1991). The difference by a factor of two between these decay times seems to be well correlated with the diameters of the rods in the two types of chlorosomes, as the rods of *Chloroflexaceae* are supposed to have half the diameter compared to the rods of *Chlorobiaceae*. The depolarization process might not be restricted to a single rod: whenever the excitation is in suitable position, it may hop to another rod, or, if the rod is in direct contact with the baseplate, also to BChl *a*. The latter case will be discussed in the following section.

Assuming the energy transfer process between these localized states is governed by Förster theory, we can estimate the ratio of the energy transfer rates between the nearest neighbors in the model aggregate:

$$\frac{k_{1-2}}{k_{1-x}} = \frac{\kappa^2_{1-2}}{\kappa^2_{1-x}} \left(\frac{r_{1-x}}{r_{1-2}}\right)^6, \qquad (1)$$

where k_{1-x} is rate constant between the dipoles 1 and $x = 2$, 3, 4, 5 (see Fig. 9 *b*), κ is the orientation factor for dipole-dipole interaction, and r is the distance between the dipoles. κ^2/r^6 values are calculated for the original and our modified models, and the results are listed in Table 4. From Table 4, one can see that for the original model (Prokhorenko et al., 2000) the most favorable direction for excitation hopping is within the stack, whereas for our modified model the highest probability of hopping is around the rod (from the dipole 1 to dipoles 3 and 4). On the other hand, the probability of the excitation delocalization is highest in the direction of the strongest coupling, i.e., within the stack for the original model and in the direction of ~10° to that of the stack for our model. The hoping time τ_{hop} between the closest sites in neighboring stacks can be calculated from an anisotropy decay time τ_{anis} using a formula given by Bradforth et al. (1995):

$$\tau_{hop} = \tau_{anis} \; 4 \; \sin^2\left(\frac{360}{N}\right) \qquad (2)$$

For number of stacks $N = 62$ and $\tau_{anis} = 15$ ps, the averaged lifetime, one gets ~615 fs for hopping time between neighboring stacks. This time would be 1.8 ps for $N =$ 36 in the original model (Prokhorenko et al., 2000).

A decay component with a 10–20 ps lifetime was resolved regardless of number of fitting parameters in isotropic decays in the red part of the BChl e Qy band. The correspondence between this component and the 10–20 ps anisotropy is manifested not only by the similar time constants, but also by the similar trend of their lifetime change with the pump-probe wavelength separation. In addition, the lifetimes associated with these two processes also have very similar pump intensity dependence, indicating that they may originate from the same process (Table 3).

BChl *e*→BChl *a* and later BChl *e*→BChl *e* energy transfer processes

The fastest process resolved in the BChl *a* region after excitation at 685 nm is characterized by ~1 ps rise observed at probe wavelengths $785 \leq \lambda_{det} < 810$ nm, which at longer wavelengths and/or higher pump intensities change into fast ESA preceding PB/SE signal. Despite its small amplitude, this component is clearly visible in the kinetics because of its short lifetime (inset of Fig. 2 *b*). Our calculated and experimental absorption spectra suggest there are no states of BChl *e* above 785 nm, and thus the possibility that this process arises from BChl *e*→BChl *e* energy transfer seems to be unlikely. Rather we believe that the process observed at low pump intensities reflects fast BChl *e*→BChl *a* energy transfer that might occur if the excitation is found in such a position on the rod with a close contact to baseplate, which enables a direct transfer to BChl *a*. The idea is supported by following reasons: 1), The lifetime of the rise is essentially identical to that of anisotropy decay at 795 nm (0.9–1.4 ps), which reflects the depolarization within BChl *a*, presumably by Förster energy transfer. Such a depolarization is observed after excitation at the blue edge of the BChl *e* band (685 nm; Fig. 8 *d*), where the probability of direct BChl *a* excitation is negligible. This means that at least part of the excitation energy (presumably ~4%; see below) is transferred from BChl *e* to BChl *a* within 1 ps. 2), Recently it was shown that there are preferentially two layers of rods in chlorosomes of *Cb. phaeobacteroides* grown under the same conditions as those used in our work (Martinez-Planells et al., 2002). For a chlorosome organization with rods hexadiagonally organized in two layers (e.g., four rods in the ground layer and three rods in an upper layer, Fig. 11), the probability that the initial excitation is in the rod with direct contact to the baseplate and will be transferred to BChl *a* is ~15% (all

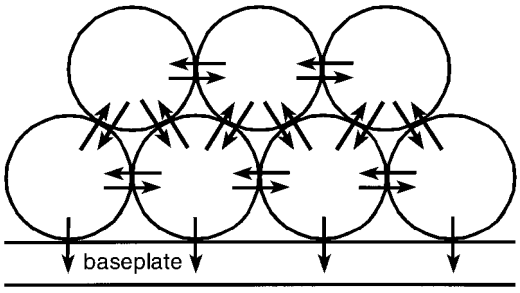

FIGURE 11 Schematic representation of the assumed main interrod and BChl $e \rightarrow$BChl a energy transfer processes within the chlorosome. For simplicity, every arrow represents event with identical probability.

probabilities of energy transfer between rods are considered to be equal and backward energy transfer from BChl a negligible, i.e., every arrow in Fig. 11 represents event with identical probability). One-quarter of these 15% represents a possibility that the excitation is in the quadrant in touch with the baseplate and the conditions for a direct transfer directly are fulfilled. This ~4% probability agrees well with the amplitude of the 1 ps rise determined in BChl a kinetics (Table 1). The presence of this direct, rapid transfer from BChl e to a may also explain one remaining discrepancy in the decay time constants measured by means of SPT and TA techniques in our previous study (Psencik et al., 2002). Using SPT, we resolved two rise components in BChl a (~30 and ~90 ps), and the faster one has dominant amplitudes between ~785–800 nm, whereas the latter had a maximal amplitude at ~815 nm. Such a spectral heterogeneity was not observed for the rise components determined using TA. The existence of ~1 ps rise component at $\lambda < 810$ nm, although it could not be resolved in SPT, would give rise to a shorter average lifetime of fluorescence in this spectral range.

In preceding section, we discussed that within 10–20 ps, the energy is completely randomized over the entire rod via a process connected also with interrod excitation hopping. In addition, excitation of the rod in direct contact with the baseplate may lead to a transfer also to BChl a. In the latter case, the isotropic decay of BChl e should have a counterpart in the rise of BChl a, as a consequence of BChl $e \rightarrow$BChl a energy transfer, which was indeed observed experimentally (lifetime of 14–20 ps). Moreover, as already mentioned, for a chlorosome with two layers of rods (Fig. 11), the probability that the initial excitation is in the rod with contact to the baseplate and will be directly transferred to BChl a is ~15%, among which ~4% are transferred before the depolarization over the rod with a 1-ps lifetime. The remaining ~11%, which are supposed to be transferred after the depolarization, corresponds well with the relative amplitude of the 18-ps rise component observed within BChl a (9–14%). In contrast, the relative amplitude of the 10–20 ps component resolved within BChl e band is clearly larger, indicating additional contribution from excitation hopping within BChl e itself. However, the absence of a corresponding rise in the red edge of BChl e band seems to be contradictory to this consideration. Possible explanation for the absence of this rise includes backward energy transfer as a result of high density of the states with energy spacing smaller than kT (see below) and/or the spectral overlap between SE of excitation donors with PB of acceptors (Savikhin et al., 1995).

The energy transfer processes discussed above require that the energy redistribution around the entire rod (1), localized excitation hopping to the neighboring rods (2), and hopping to the BChl a in close vicinity (3), should occur with similar lifetimes, which are indistinguishable experimentally. Although similarity of the lifetimes belonging to (1) and (3) was directly observed in our experiments, for the lifetime of the process (2), we have only indirect experimental evidence. However, additional support was obtained from the numerical modeling described in the next paragraph.

The major BChl e deexcitation, as seen from three-component fits, occurs with a lifetime of ~80–100 ps. On the basis of following arguments, we believe that this time scale represents the relaxation of excitation equilibrated over BChl e of a whole chlorosome. 1), Because there is no experimental evidence to support the presence of different spectral pools in this specific chlorosomes (see below), we consider that all the rods are spectrally indistinguishable. In this case, it is reasonable to consider that the energy transfer between rods does not proceed in any specific direction, for instance, toward the baseplate; rather, it has an equal probability of transfer to any neighboring rod or BChl a (Fig. 11). Therefore, the overall BChl e decay can be significantly slower than the 10–20 ps lifetime connected with the excitation depolarization. Such a behavior was modeled numerically by considering several rods with an interrod energy transfer time of 15 ps. Depending on the number of rods (7–9) and their arrangement, the overall decay and a rise in an acceptor pool (BChl a) were found to be equal, characterized by a time constant of ~40–120 ps. 2), The high number of pigments in chlorosomes gives rise to a high density of energy levels. Energy transfer processes between those states with relatively small energy differences may be invisible for our isotropic measurements, as far as it is within the detection window of the probe pulse. 3), At room temperature, the thermal energy is ~200 cm^{-1}, corresponding to ~10 nm in the spectral region of interest. The presence of high density of states will give rise to uphill energy transfer, which may exceed the spectral range covered by the probe pulse. This process will again effectively obscure individual energy transfer step within the chlorosome. The transient spectra measured at low pump intensities (not shown) indicate that the equilibrium within a chlorosome is reached very fast: all the shifts and broadening complete within 1 ps. This can be understood as a dynamic equilibrium when all the uphill and downhill

processes within the BChl *e* manifold and the forward and the backward energy transfer between the rods are in balance. Therefore the main component of the BChl *e* decay observed at respective probe wavelength can be interpreted as an enveloping relaxation process of equilibrated BChl *e* pool or at least of its part within the detection window of the probe pulse.

The main part of excitation arrives at the baseplate with a timescale of ~120–130 ps, resolved from the rise of the BChl *a*. In contrast to the ~18 ps component, this ~125 ps rise time does not match the lifetime of the corresponding main decay component in BChl *e*. It suggests that this transfer step is not a direct process. Although one could force the time constant of the decay and the rise to be identical using global lifetime analysis with a model function consisting of four exponentials, this analysis results in a noticeable worse χ^2 (see Results). In addition, the satisfactory fitting of individual kinetics indicates that the difference in the lifetimes of the major decay and rise of BChl *e* and a, respectively, may be an inherent feature of this particular chlorosomes.

We will now focus on discussing the possible origin of this difference in the decay and rise lifetimes. To this end, we first note that the difference between the lowest exciton levels of BChl *e* and BChl *a* transitions is sufficiently large to prohibit any significant backward energy transfer from BChl *a*→BChl *e* at room temperature (as judged from the DAS or the calculated spectra). The alternative possibility is the existence of a second BChl *e* pool, where at least a portion of energy is accumulated before the transfer to BChl *a*. Such a pool can be formed by a different, long-wavelength absorbing spectral form of BChl *e* or by the lowest exciton levels.

Existence of multiple spectral pools was proposed for the chlorosomes of various green bacteria, such as the one containing more than one chlorosomal BChl species (Steensgaard et al., 2000b). For the chlorosomes containing single aggregated BChl, the evidence that supports multiple spectral forms includes the second derivatives of absorption and fluorescence spectra or orientation changes observed in CD and LD (for references, see Introduction). It was often assumed that these spectral pools are spatially arranged in such a way that it will enhance the energy transfer toward the baseplate. For the chlorosomes from *Cb. phaeobacteroides* used in the current work, the second derivatives of the absorption and the fluorescence spectra, as well as the fluorescence anisotropy and the CD spectrum, do not provide any hint for the existence of different BChl *e* spectral forms. In addition, the measurements of the TA kinetics also indicate a high spectral homogeneity of both BChl *e* and BChl *a* pools. In this regard, we note that the kinetics measured within BChl *a* are very similar, irrespective of the pump and probe wavelengths, and the differences between the kinetics detected within BChl *e* are mainly due to the wavelength-dependent contribution from the exciton relaxation. In addition, the BChl *e* kinetics measured between 725 and 755 nm exhibit similar amplitude ratio between the ~18 and ~80 ps decay components.

The only evidence supporting the spectral inhomogeneities for the chlorosomes under investigation is the observation of a local maximum at ~770 nm in the DAS obtained from SPT measurements (Psencik et al., 2002). This wavelength is close to the maximum of the lowest exciton levels distribution function calculated for the disordered aggregates in this work and also to the emission maxima of BChl *e* in chlorosomes at low temperatures (not shown). As the energies of these states are too low to allow efficient uphill energy transfer even at room temperature and, in addition, their density of state is relatively low, it therefore will enhance the probability of deexcitation via spontaneous emission, despite their small oscillator strength. Inasmuch as the probability of emission from the higher energy states is limited due to their short lifetime, this may lead to the occurrence of the local maximum in the DAS. In this case, the lowest exciton levels will effectively show up as a separate pool due to their longer lifetime, although actually they are not a spatially discrete pool. The presence of these long-lived, lowest exciton states is supported by the exceptionally slow decay components (with lifetimes exceeding even the decay time observed in the BChl *a* region) and relatively large amplitudes, as resolved at 765 and 775 nm (see Table 1). As the number of these long-lived states increases with the wavelength, it can readily explain the increase of the rise times with increasing pump wavelength, resolved at a given probe wavelength within BChl *a* (see Table 2). Furthermore, this can explain the discussed difference in the decay and rise lifetime: the main rise component in the BChl *a* is expected to be contributed by the main decay component of BChl *e*, which was 80–100 ps at the wavelengths $\lambda_{det} \leq 755$ nm (as resolved from the three-component fits), but significantly slower at around 765 nm, where the lowest exciton levels contribute. Weighted averaging of all these decays will therefore lead to the slower rise in BChl *a* compared to the 80–100 ps decay observed at most wavelengths within BChl *e*. To conclude, although the lowest exciton levels have dominant contribution to the spontaneous emission in comparison to the higher lying states, they may act effectively as a bottleneck, preventing partly the escape of excitation from the energy transfer pathway as the result of their small oscillator strength and consequently longer lifetimes. Contribution of these states results in the observed slower rise in BChl *a* compared to the dominating decay in the main BChl *e* region. Such a behavior could be simulated also numerically. We believe that such an interpretation is plausible to the various chlorosomes in general, and, in particular, it was indeed one of the alternatives proposed to explain occurrence of a second BChl *c* pool, denoted E790, for *Cb. limicola* (Steensgaard et al., 2000b). Generally, the lowest states differ from the upper exciton levels by their energy, lifetime, and dipole orientation (due to their localized character), and these symptoms could

lead to the attribution of these states as a different spectral form of a given BChl species in some cases.

CONCLUSIONS

The huge number of molecules in the chlorosomal aggregates results in the onset of excitation annihilation at remarkable low pump intensity in comparison to any other light-harvesting antenna complexes ever found. To reveal the energy transfer processes of interest, it is crucial to carry out measurements under the annihilation-free conditions, which, for this particular chlorosome preparation, require pump intensity in the order of 10^{11} photons $\times$ pulse^{-1} $\times$ cm^{-2}. Our measurements under the annihilation-free conditions lead to several new observations, and among them, the most prominent ones are the fast rise in the BChl *e* and the considerably slow anisotropy decays. The interpretation of the experimental data is based on the modification of the original model proposed by Holzwarth and Schaffner (1994), in which the direction of the BChl *e* Q_y transition dipole moment is altered in accordance with results of various experiments. This modification results in a redistribution of the main oscillator strength from the lowest exciton levels to higher lying states and an overall increase of interaction energies, leading to a good agreement between experimental and calculated absorption and CD spectra. In addition, the obtained energy difference between main absorbing states, with orientation of their dipoles close to parallel to the aggregate axis, and the lowest levels, with average orientation close to that of individual BChl molecules, enables to explain the large Stokes shift between absorption and fluorescence. We found experimentally that excitation of the higher exciton levels is followed by fast exciton relaxation with timescale of 200–500 fs, finally leading to population of low-lying states with a highly localized character, from which further energy transfer steps occur. The internal conversion from the Soret band is even faster. The anisotropy decays relatively slowly within BChl *e* manifold (10–20 ps), and it is attributed to the redistribution of the excitation around the rod, corresponding to a hopping time of ~600 fs between the stacks. This redistribution process may also lead to the transfer to the neighboring aggregate (rod) and/or to the baseplate BChl *a*, provided that the excitation finds itself at suitable position. This leads to the occurrence of a minor decay and rise component in the BChl *e* and BChl *a* spectral regions, respectively, with a more or less identical lifetime as the anisotropy decay. The major portion of excitation arrives to the baseplate with a timescale of 120–130 ps, which is remarkably longer than the time constant associated with the main decay component (80–100 ps) observed at most wavelengths within BChl *e* manifold. The difference is attributed to the contribution of the long-lived lowest exciton levels, which results in the slowdown of overall excitation transfer to the BChl *a*. The energy transfer between BChl *a* molecules was determined to have ~1 ps lifetime on the basis of anisotropy decay, which is similar to the shortest of three resolved BChl *e*→BChl *a* energy transfer steps. In general, the proposed scheme of intrachlorosomal energy transfer processes might be applicable also for other green bacteria, inasmuch as qualitatively similar results were obtained also for BChl *c* containing chlorosomes of *Cb. tepidum* (unpublished data).

APPENDIX

Optical spectra were calculated in a point-dipole approximation by taking into account only Q_y transitions. All interactions between the transition dipoles were considered. An electronic Hamiltonian for the Frenkel exciton was used (Davydov, 1971; Pullerits, 2000)

$$\mathsf{H} = \sum_{i,j}(\mathsf{E} + \mathsf{D}_i + \Delta_i)\langle i|i\rangle + \mathsf{V}_{ij}\langle i|\,j\rangle, \tag{3}$$

where E is the electronic transition energy of the noninteracting monomer, D_i is the solvent shift (also the spectral shifts caused by hydrogen bonding are included in this term), and Δ_i is an origin of inhomogeneous broadening: a random shift from the average energy $\nu_i = E + D_i$ caused by stochastic fluctuations in the environment of the ith molecule (Pullerits, 2000). As all molecules forming the aggregate are involved in the identical hydrogen bonding (with exception of those at the edges), we assume that D_i is nearly constant for all pigments within the chlorosome. Because the value of D is unknown, we set it to zero in our calculations, and, as this parameter usually leads to a red shift (van Amerongen et al., 2000), the choice of zero value for D in our calculation is compensated by using low values of dielectric constant (1.0–1.1; i.e., close to the vacuum value) (Eq. 4). The actual value of the dielectric constant in chlorosomes is undefined yet; however, as the chlorosome aggregates contain nearly no protein, its value is expected to be significantly lower than that in a protein environment (typically $\varepsilon = 2$ is used). Δ_i was introduced by assuming a Gaussian distribution of molecular energies (diagonal energetic disorder). Nondiagonal energetic disorder was omitted because it has only a small effect on the spectra (Pullerits, 2000). The dipole-dipole interaction V_{ij} (in cm^{-1}) between electronic transition dipole moments is given by

$$\mathsf{V}_{ij} = \frac{5.04}{\varepsilon}\left[\frac{\vec{\boldsymbol{\mu}}_i \cdot \vec{\boldsymbol{\mu}}_j}{\mathsf{r}_{ij}^3} - \frac{3(\vec{\mathbf{r}}_{ij} \cdot \vec{\boldsymbol{\mu}}_i)(\vec{\mathbf{r}}_{ij} \cdot \vec{\boldsymbol{\mu}}_j)}{\mathsf{r}_{ij}^5}\right] = \left[\frac{5.04\kappa_{ij}\mu_i\mu_j}{\varepsilon \mathsf{r}_{ij}^3}\right], \tag{4}$$

where ε is dielectric constant and $\vec{\boldsymbol{\mu}}_i$ is the transition dipole moment in vacuum (in Debye) and $\vec{r}_{ij}$ is the vector connecting centers of ith and jth BChl molecule (in nm). The orientation κ_{ij} factor for the dipole-dipole interaction is important for Förster energy transfer, whose rate is proportional to κ^2 and inversely to r^6.

The exciton components of absorption and CD spectra has been calculated according to Pearlstein (1991)

$$\mu_k^2 = \sum_{i,j}^{n}(\vec{\boldsymbol{\mu}}_i \cdot \vec{\boldsymbol{\mu}}_j)\mathsf{U}_{ik}\mathsf{U}_{jk} \tag{5}$$

$$\mathcal{R}_k = 1.7 \times 10^{-5}\sum_{i,j}^{n}\nu_i[\vec{\mathbf{r}}_{ij} \cdot (\vec{\boldsymbol{\mu}}_j \times \vec{\boldsymbol{\mu}}_i)]\mathsf{U}_{ik}\mathsf{U}_{jk}, \tag{6}$$

where $\mathcal{R}_k$ is rotational strength (in Debye-Bohr magnetons) and U_{ik} and U_{jk} are corresponding eigenvectors, and ν_i is energy of the transition on the ith molecule. The components of fluorescence spectra were obtained by weighting of the absorption components by a Boltzmann factor.

$$\mathsf{F}_k = \mu_k^2 \exp\left(-\frac{\mathsf{e}_k}{\mathsf{kT}}\right), \tag{7}$$

where e_k is the energy of corresponding absorption component. The formula assumes that emission occurs after exciton relaxation from levels populated according to the Boltzmann law.

Position vectors $\vec{r}_{ij}$ and the orientation of the dipole moments $\vec{\mu}_i$ were derived from structural parameters of the original model (Holzwarth and Schaffner, 1994; Prokhorenko et al., 2000). Following distribution of dipoles was used:

$$r_i = \begin{vmatrix} R\ \sin\alpha_i \\ R\ \cos\alpha_i \\ z_i \end{vmatrix} \quad \hat{\mu}_i = \begin{vmatrix} \sin\gamma\ \cos(\alpha_i + \beta) \\ \sin\gamma\ \sin(\alpha_i + \beta) \\ \cos\gamma \end{vmatrix}$$
$$i = 1, 2 \ldots n, \tag{8}$$

where α and z are cylindrical coordinates. The third cylindrical coordinates, R, was kept constant and is equal to the assumed radius of the rod ($\sim$5 nm). β is the angle between position vector r_i and the projection of transition moment into the $R\alpha$ plane, and γ is the angle between the transition moment and symmetry axis (z) of the aggregate.

In the calculations, an energy of 15 125 cm^{-1} was used for the Q_y transition of monomeric BChl *e*, and the value of the dipole strength was chosen to be 23 $Debye^2$ (lower bound of the estimate; Arellano et al., 2000). Interactions between rods were not considered. The other parameters used for particular calculations are given in corresponding figure legends. The structural parameters are listed in Table 4, except $\beta = 95°$ (insensitive to small changes) and $\gamma = 20°$.

This research was supported by the Swedish Natural Science Research Council, the European Union Training and Mobility of Researchers project ''Green Bacterial Photosynthesis'' (grant FMRX-CT96-0081), and the Kempe Foundation. J. Pšenčík also thanks the Swedish Institute and Grant Agency of the Czech Republic (grant 206/02/0942) for financial support.

REFERENCES

Alden, R. G., S. H. Lin, and R. E. Blankenship. 1992. Theory of spectroscopy and energy transfer of oligomeric pigments in chlorosome antennas of green photosynthetic bacteria. *J. Lumin.* 51:51–66.

Arellano, J. B., J. Psencik, C. M. Borrego, Y. Z. Ma, R. Guyoneaud, J. Garcia-Gil, and T. Gillbro. 2000. Effect of carotenoid biosynthesis inhibition on the chlorosome organization in Chlorobium phaeobacteroides strain CL1401. *Photochem. Photobiol.* 71:715–723.

Balaban, T. S., A. R. Holzwarth, K. Schaffner, G. J. Boender, and H. J. de Groot. 1995. CP-MAS ^{13}C-NMR dipolar correlation spectroscopy of ^{13}C-enriched chlorosomes and isolated bacteriochlorophyll *c* aggregates of Chlorobium tepidum: the self organization of pigments is the main structural feature of chlorosomes. *Biochemistry*. 34:15259–15266.

Blankenship, R. E., J. M. Olson, and M. Miller. 1995. Antenna complexes from green photosynthetic bacteria. *In* Anoxygenic Photosynthetic Bacteria. R. E. Blankenship, M. T. Madigan, and J. Bautista, editors. Kluwer Academic Publisher, Dordrecht, The Netherlands. 399–435.

Boender, G. J., T. S. Balaban, A. R. Holzwarth, K. Schaffner, J. Raap, S. Prytulla, H. Oschkinat, and H. J. de Groot. 1995. Comparison of the stacking of chlorophylls in chlorosomes versus aggregates of bacteriochlorophyll *c* and chlorophyll *a* using 2-D NMR spectroscopy. *In* Photosynthesis: From Light to Biosphere, Vol. 1. P. Mathis, editor. Kluwer Academic Publisher, Dordrecht, The Netherlands. 347–350.

Bradforth, S. E., R. Jimenez, F. van Mourik, R. van Grondelle, and G. R. Fleming. 1995. Excitation transfer in the core light-harvesting complex (LH-1) of Rhodobacter sphaeroides. An ultrafast fluorescence depolarization and annihilation study. *J. Phys. Chem.* 99:16179–16191.

Buck, D. R., and W. S. Struve. 1996. Tubular exciton model for BChl *c* antennae in chlorosomes from green photosynthetic bacteria. *Photosynth. Res.* 48:367–377.

Carbonera, D., E. Bordignon, G. Giacometti, G. Agostini, A. Vianelli, and C. Vannini. 2001. Fluorescence and absorption detected magnetic resonance of chlorosomes from green bacteria Chlorobium tepidum and Chloroflexus aurantiacus. A comparative study. *J. Phys. Chem. B.* 105:246–255.

Causgrove, T. P., D. C. Brune, J. Wang, B. P. Wittmershaus, and R. E. Blankenship. 1990. Energy transfer in whole cells and isolated chlorosomes of green photosynthetic bacteria. *Photosynth. Res.* 26:39–48.

Causgrove, T. P., D. C. Brune, and R. E. Blankenship. 1992. Förster energy transfer in chlorosomes of green photosynthetic bacteria. *J. Photochem. Photobiol.* 15:171–179.

Chiefari, J., K. Griebenow, F. Fages, N. Griebenow, T. S. Balaban, A. R. Holzwarth, and K. Schaffner. 1995. Models for the pigment organization in the chlorosomes of photosynthetic bacteria. Diastereoselective control of in vivo bacteriochlorophyll c_s aggregation. *J. Phys. Chem.* 99:1357–1365.

Davydov, A. S. 1971. Theory of Molecular Excitons. Plenum, New York.

Fetisova, Z. G., S. G. Kharchenko, and I. A. Abdourakhmanov. 1986. Strong orientational ordering of the near-infrared transition-moment vectors of light-harvesting antenna bacterioviridin in chromatophores of the green photosynthetic bacterium Chlorobium limicola. *FEBS Lett.* 199:234–236.

Fetisova, Z. G., and K. Mauring. 1992. Experimental evidence of oligomeric organization of antenna bacteriochlorophyll *c* in green bacterium Chloroflexus aurantiacus by spectral hole burning. *FEBS Lett.* 307:371–374.

Fetisova, Z. G., A. Freiberg, K. Mauring, V. I. Novoderezhkin, A. S. Taisova, and K. Timpmann. 1996. Excitation energy transfer in chlorosomes of green bacteria: theoretical and experimental studies. *Biophys. J.* 71:995–1010.

Frese, R., U. Oberheide, I. van Stokkum, R. van Grondelle, M. Foidl, J. Oelze, and H. van Amerongen. 1997. The organization of bacteriochlorophyll *c* in chlorosomes from Chloroflexus aurantiacus and the structural role of carotenoids and protein. An absorption, linear dichroism, circular dichroism, and Stark spectroscopy study. *Photosynth. Res.* 54:115–126.

Frigaard, N. U., S. Takaichi, M. Hirota, K. Shimada, and K. Matsuura. 1997. Quinones in chlorosomes of green sulfur bacteria and their role in the redox-dependent fluorescence studied in chlorosome-like bacteriochlorophyll *c* aggregates. *Arch. Microbiol.* 167:343–349.

Griebenow, K., A. R. Holzwarth, F. van Mourik, and R. van Grondelle. 1991. Pigment organization and energy transfer in green bacteria. 2. Circular and linear dichroism spectra of protein-containing and protein-free chlorosomes isolated from Chloroflexus aurantiacus strain Ok-70-fl. *Biochim. Biophys. Acta.* 1058:194–202.

Hildebrandt, P., K. Griebenow, A. R. Holzwarth, and K. Schaffner. 1991. Resonance Raman spectroscopic evidence for the identity of the bacteriochlorophyll *c* organisation in protein-free and protein-containing chlorosomes from Chloroflexus aurantiacus. *Z Naturforsch.* 46c:228–232.

Holzwarth, A. R., M. G. Müller, and K. Griebenow. 1990. Picosecond energy transfer kinetics between pools in different preparations of chlorosomes from the green bacterium Chloroflexus aurantiacus Ok-70-fl. *J. Photochem. Photobiol.* 5:457–465.

Holzwarth, A. R., and K. Schaffner. 1994. On the structure of bacteriochlorophyll molecular aggregates in the chlorosomes of green bacteria. A molecular modelling study. *Photosynth. Res.* 41:225–233.

Lin, S., H. van Amerongen, and W. S. Struve. 1991. Ultrafast pump-probe spectroscopy of bacteriochlorophyll *c* antenna in bacteriochlorophyll *a*-containing chlorosomes from the green photosynthetic bacterium Chloroflexus aurantiacus. *Biochim. Biophys. Acta.* 1060:13–24.

Ma, Y. Z., R. P. Cox, T. Gillbro, and M. Miller. 1996. Bacteriochlorophyll organization and energy transfer kinetics in chlorosomes from Chloroflexus aurantiacus depend on the light regime during growth. *Photosynth. Res.* 47:157–165.

Ma, Y. Z., R. J. Cogdell, and T. Gillbro. 1997. Energy transfer and exciton annihilation in the B800-850 antenna complex of the photosynthetic purple bacterium Rhodopseudomonas acidophila (Strain 10050). A femtosecond transient absorption study. *J. Phys. Chem. B.* 101:1087–1095.

Ma, Y. Z., R. J. Cogdell, and T. Gillbro. 1998. Femtosecond energy-transfer dynamics between bacteriochlorophylls in the B800-820 antenna complex of the photosynthetic purple bacterium Rhodopseudomonas acidophila (Strain 7750). *J. Phys. Chem. B.* 102:881–887.

Martinez-Planells, A., J. B. Arellano, C. A. Borrego, C. Lopez-Iglesias, F. Gich, and J. S. Garcia-Gil. 2002. Determination of the topography and biometry of chlorosomes by atomic force microscopy. *Photosynth. Res.* 71:83–90.

Melo, T. B., N. U. Frigaard, K. Matsuura, and K. R. Naqvi. 2000. Electronic energy transfer involving carotenoid pigments in chlorosomes of two green bacteria: Chlorobium tepidum and Chloroflexus aurantiacus. *Spectrochim Acta A Mol. Biomol Spectrosc.* 56:2001–2010.

Miller, M., R. P. Cox, and T. Gillbro. 1991. Energy transfer kinetics in chlorosomes from Chloroflexus aurantiacus: studies using picosecond absorbance spectroscopy. *Biochim. Biophys. Acta.* 1057:187–194.

Mimuro, M., Y. Nishimura, I. Yamazaki, M. Kobayashi, Z. Y. Wang, T. Nozawa, K. Shimada, and K. Matsuura. 1996. Excitation energy transfer in the green photosynthetic bacterium Chloroflexus aurantiacus: a specific effect of 1-hexanol on the optical properties of baseplate and energy transfer processes. *Photosynth. Res.* 48:263–270.

Olson, J. M. 1998. Chlorophyll organization and function in green photosynthetic bacteria. *Photochem. Photobiol.* 67:61–75.

Overmann, J., H. Cypionka, and N. Pfennig. 1992. An extremely low-light-adapted phototrophic sulfur bacterium from the Black Sea. *Limnology and Oceanography.* 37:150–155.

Pearlstein, R. M. 1991. Theoretical interpretation of antenna spectra. *In* Chlorophylls. H. Scheer, editor. CRC Press, Boca Raton, FL, USA. 1047–1077.

Prokhorenko, V. I., D. B. Steensgaard, and A. F. Holzwarth. 2000. Exciton dynamics in the chlorosomal antennae of the green bacteria Chloroflexus aurantiacus and Chlorobium tepidum. *Biophys. J.* 79:2105–2120.

Psencik, J., G. F. W. Searle, J. Hala, and T. J. Schaafsma. 1994a. Fluorescence-detected magnetic-resonance (FDMR) of green sulfur photosynthetic bacteria Chlorobium sp. *Photosynth. Res.* 40:1–10.

Psencik, J., M. Vacha, F. Adamec, M. Ambroz, J. Dian, J. Bocek, and J. Hala. 1994b. Hole-burning study of excited-state structure and energy-transfer dynamics of bacteriochlorophyll *c* in chlorosomes of green sulfur photosynthetic bacteria. *Photosynth. Res.* 42:1–8.

Psencik, J., T. J. Schaafsma, G. W. Searle, and J. Hala. 1997. Fluorescence detected magnetic resonance of monomers and aggregates of bacteriochlorophylls of green sulfur bacteria Chlorobium sp. *Photosynth. Res.* 52:83–92.

Psencik, J., T. Polivka, P. Nemec, J. Dian, J. Kudrna, P. Maly, and J. Hala. 1998. Fast energy transfer and exciton dynamics in chlorosomes of the green sulfur bacterium Chlorobium tepidum. *J. Phys. Chem. A.* 102:4392–4398.

Psencik, J., Y. Z. Ma, J. B. Arellano, J. Garcia-Gil, A. R. Holzwarth, and T. Gillbro. 2002. Excitation energy transfer in chlorosomes of Chlorobium phaeobacteroides strain CL1401: the role of carotenoids. *Photosynth. Res.* 71:5–18.

Pullerits, T. 2000. Exciton states and relaxation in molecular aggregates: numerical study of photosynthetic light harvesting. *J. Chin. Chem. Soc.* 47:773–784.

Savikhin, S., Y. Zhu, S. Lin, R. E. Blankenship, and W. S. Struve. 1994. Femtosecond spectroscopy of chlorosome antennas from the green photosynthetic bacterium Chloroflexus aurantiacus. *J. Phys. Chem.* 98:10322–10334.

Savikhin, S., P. I. van Noort, Y. Zhu, S. Lin, R. E. Blankenship, and W. S. Struve. 1995. Ultrafast energy transfer in light-harvesting chlorosomes from the green sulfur bacterium Chlorobium tepidum. *Chem. Phys.* 194:245–258.

Savikhin, S., Y. Zhu, R. E. Blankenship, and W. S. Struve. 1996a. Intraband energy transfers in the BChl *c* antenna of chlorosomes from the green photosynthetic bacterium Chloroflexus aurantiacus. *J. Phys. Chem.* 100:17978–17980.

Savikhin, S., Y. Zhu, R. E. Blankenship, and W. S. Struve. 1996b. Ultrafast energy transfer in chlorosomes from the green photosynthetic bacterium Chloroflexus aurantiacus. *J. Phys. Chem.* 100:3320–3322.

Savikhin, S., D. R. Buck, W. S. Struve, R. E. Blankenship, A. S. Taisova, V. I. Novoderezhkin, and Z. G. Fetisova. 1998. Excitation delocalization in the bacteriochlorophyll *c* antenna of the green bacterium Chloroflexus aurantiacus as revealed by ultrafast pump-probe spectroscopy. *FEBS Lett.* 430:323–326.

Somsen, O. J., R. van Grondelle, and H. van Amerongen. 1996. Spectral broadening of interacting pigments: polarized absorption by photosynthetic proteins. *Biophys. J.* 71:1934–1951.

Steensgaard, D. B., H. Wackerbarth, P. Hildebrandt, and A. R. Holzwarth. 2000a. Diastereoselective control of bacteriochlorophyll *e* aggregation. 3(1)-S-BChl *e* is essential for the formation of chlorosome-like aggregates. *J. Phys. Chem. B.* 104:10379–10386.

Steensgaard, D. B., C. A. van Walree, H. Permentier, L. Baneras, C. M. Borrego, J. Garcia-Gil, T. J. Aartsma, J. Amesz, and A. R. Holzwarth. 2000b. Fast energy transfer between BChl *d* and BChl *c* in chlorosomes of the green sulfur bacterium Chlorobium limicola. *BBA-Bioenergetics.* 1457:71–80.

van Amerongen, H., H. Vasmel, and R. van Grondelle. 1988. Linear dichroism of chlorosomes from *Chloroflexus aurantiacus* in compressed gels and electric fields. *Biophys. J.* 54:65–76.

van Amerongen, H., B. van Haeringen, M. van Gurp, and R. van Grondelle. 1991. Polarized fluorescence measurements on ordered photosynthetic antenna complexes. *Biophys. J.* 59:992–1001.

van Amerongen, H., L. Valkunas, and R. van Grondelle. 2000. Photosynthetic Excitons. World Scientific, Singapore.

van Noort, P. I., Y. Zhu, R. LoBrutto, and R. E. Blankenship. 1997. Redox effects on the excited-state lifetime in chlorosomes and bacteriochlorophyll *c* oligomers. *Biophys. J.* 72:316–325.

van Rossum, B. J., D. B. Steensgaard, F. M. Mulder, G. J. Boender, K. Schaffner, A. R. Holzwarth, and H. M. de Groot. 2001. A refined model of the chlorosomal antennae of the green bacterium Chlorobium tepidum from proton chemical shift constraints obtained with high-field 2-D and 3-D MAS NMR dipolar correlation spectroscopy. *Biochemistry.* 40:1587–1595.

van Walree, C. A., Y. Sakuragi, D. B. Steensgaard, N. U. Frigaard, R. P. Cox, A. R. Holzwarth, and M. Miller. 1999. Effect of alkaline treatment on bacteriochlorophyll *a*, quinones and energy transfer in chlorosomes from Chlorobium tepidum and Chlorobium phaeobacteroides. *Photochem. Photobiol.* 69:322–328.

Wang, J., D. C. Brune, and R. E. Blankenship. 1990. Effects of oxidants and reductants on the efficiency of excitation transfer in green photosynthetic bacteria. *Biochim. Biophys. Acta.* 1015:457–463.